Adventitial Cell Atlas of Wild-type and ApoE-deficient Mice Defined by Single-cell RNA-sequencing

Wenduo Gu, Zhichao Ni, Yuan-Qing Tan, Jiacheng Deng, Si-Jin Zhang, Zi-Chao Lv, Xiao-Jian Wang, Ting Chen, Zhongyi Zhang, Yanhua Hu, Zhi-Cheng Jing, and Qingbo Xu

School of Cardiovascular Medicine and Sciences, King's College London BHF Centre (W.G., Z.N., J.D., Y.H., Q.X.), London, United Kingdom; Key Lab of Pulmonary Vascular Medicine & FuWai Hospital, State Key Laboratory of Cardiovascular Disease, Peking Union Medical College and Chinese Academy Medical Sciences (YQ.T., SJ.Z., ZC.Lv., XJ. W., ZC.J.), Beijing, China; Department of Cardiology, The First Affiliated Hospital, Zhejiang University, Zhejiang, China (T.C., Q.X.).

Running title: Adventitial cell atlas

Subject terms:

Single-cell RNA-sequencing, Cell atlas, Vascular biology, Atherosclerosis

Word counts: 7,290

Figures: 8

Correspondence to

Qingbo Xu, MD, PhD, School of Cardiovascular Medicine & Sciences, King's College London BHF Centre, 125 Coldharbour Lane, London SE5 9NU, United Kingdom Telephone: (+44) 20 7848-5322, Fax: (+44) 20 7848-5296, Email: qingbo.xu@kcl.ac.uk

or Zhi-cheng Jing, MD, Key Lab of Pulmonary Vascular Medicine & FuWai Hospital, State Key Laboratory of Cardiovascular Disease, Peking Union Medical College and Chinese Academy Medical Sciences, No. 167 Beilishi Road, Beijing, 100037, China, Tel: (+86)10-88396018, Fax: (+86)10-88396016, Email: jingzhicheng@vip.163.com

Abstract

Objective: Vascular adventitia encompasses progenitors and is getting recognized as the major site of inflammation in early stage of atherosclerosis. However, the cellular atlas of the heterogeneous adventitial cells, the intercellular communication, the cellular response of adventitia to hyperlipidemia and its contribution to atherosclerosis have been elusive.

Approach and results: Single-cell RNA-sequencing was applied to wild-type and ApoE-deficient aortic adventitia from 12-week-old C57BL/6J mice fed on normal laboratory diet with early stage of atherosclerosis. Unbiased clustering analysis revealed that the landscape of adventitial cells encompassed adventitial mesenchyme cells, immune cells (macrophages, T cells and B cells) and some types of rare cells, e.g. neuron, lymphatic endothelial cells and innate lymphoid cells. Seurat clustering analysis singled out 6 non-immune clusters with distinct transcriptomic profiles, in which there predominantly were stem/progenitor cell-like and pro-inflammatory population (Mesen II). In ApoE-deficient adventitia, resident macrophages were activated and related to increased myeloid cell infiltration in the adventitia. Cell communication analysis further elucidated enhanced interaction between a mesenchyme cluster and inflammatory macrophages in ApoE-deficient adventitia. *In vitro* trans-well assay confirmed the pro-inflammatory role of $SCA1^{+}$ Mesen II population with increased CCL2 secretion and thus increased capacity to attract immune cells in ApoE-deficient adventitia.

Conclusions: Cell atlas defined by single-cell RNA-sequencing depicted the heterogeneous cellular landscape of the adventitia and uncovered several types of cell populations. Furthermore, resident cell interaction with immune cells appears crucial at the early stage of atherosclerosis.

Keywords: Adventitia, single-cell RNA-sequencing, cell atlas, cellular communication, atherosclerosis

Nonstandard Abbreviations and Acronyms:

ApoE	apolipoprotein E
DAPI	4′,6-diamidino-2-phenylindole
ECM	extracellular matrix
GO	gene ontology
GOBP	gene ontology biological pathway
GOMF	gene ontology molecular function
ILC	Innate lymphoid cell
KEGG	Kyoto encyclopedia of genes and genomes
NK	natural killer
SMC	smooth muscle cell
scRNA-seq	single-cell RNA-sequencing
TOM	topological overlap matrix
t-SNE	t-distributed stochastic neighboring embedding
UMI	unique molecular identifier
WGCNA	weighted gene co-expression network analysis
wt	wild-type

Introduction

Atherosclerosis is characterized by vascular inflammation and represents a major mortality cause worldwide.[1] Traditional "inside-out" theory of atherosclerotic lesion development encompasses macrophage adhesion on the luminal surface, endothelial dysfunction, leukocyte accumulation in sub-endothelial space, and subsequent inflammatory responses.[1] These orchestrating mechanisms are established to initiate from the luminal side of the vessel. However, substantial evidence emerges and supports the "outside-in" theory.[2-4] Events in the adventitia such as angiogenesis and inflammatory infiltration correlate with plaque development.[5-7] Various cell types that reside in the dynamic adventitia including adventitial progenitors[8], myofibroblasts and immune cells have been demonstrated to participate in vascular remodeling and contribute to atherosclerotic lesion development.[4, 9, 10] It has been demonstrated that adventitia plays a key role in the development of neointima after vessel injury.[11-13] However, approaches to define adventitial progenitors and immune cells which rely on limited and pre-selected markers do not necessarily reflect their in *vivo* diversity and heterogeneity.[8] In addition, essential information about gene coordination is neglected due to the biased choices of genes to study. Adding another layer of complexity to the adventitial involvement in atherosclerosis, multiple cell types might interact and operate in concert to modulate lesion progress, and systemic study of cell communication has not been viable.

Single-cell RNA-sequencing (scRNA-seq) offers an opportunity to unbiasedly interrogate thousands of genes simultaneously at an unprecedently high resolution. Depiction of adventitial cell landscape with scRNA-seq is imperative in characterizing the cellular heterogeneity, unraveling cellular identities, uncovering underlying disease-associated markers or cells and shedding light on the potential cell communication mechanisms. Here, we performed scRNA-seq of aortic adventitial cells from wild-type (wt) and ApoE$^{-/-}$ mice to explore their heterogenous identities, diverse functional states, dynamic cellular communications and altered transcriptomic profiles in disease.

Materials and Methods

The data that support the findings of this study are available from the corresponding author upon reasonable request.

Mice and Adventitial Cell Isolation

Twelve-week-old male wt and ApoE$^{-/-}$ mice (C57BL/6J background, Jackson's Lab) were fed on normal laboratory diet. To avoid data variation incurred by sex difference[14], only male mice were selected for the study. Mice were sacrificed with cervical dislocation. Perfusion was performed with 5 ml PBS through left ventricular puncture until the liver yields a pale color. Aorta (including aortic arch, thoracic aorta and abdominal aorta) was pooled from 20 mice in each group (wt and ApoE$^{-/-}$). Adventitia was carefully peeled off from the media and intimal layer for subsequent enzyme digestion. To obtain single cells, the pooled adventitia was washed with PBS three times and then subjected with enzyme digestion with 5 ml 2 mg/ml Collagenase I (Invitrogen, 17018-029) and 2 mg/ml dispase II (Sigma, D4693) in Hank's balanced salt containing calcium and magnesium for 30 mins. All procedures involving animals in the study follow the guidelines from Directive 2010/63/EU of the European Parliament on the protection of animals. Protocols from the Institutional Committee for Use and Care of Laboratory Animal and License issued by the Home Office UK were followed.

Cell Sorting

Digested cells were filtered with 40 um filter (Corning) and then centrifuged at 300g for 5 mins. Cells resuspended in PBS were stained with LIVE/DEAD ™ Fixable Near- IR (APC/Cy7 channel) Dead Cell Stain Kit (Invitrogen, L34975, 1:1000) and Hoechst 33342 (Invitrogen, H3570, 1:1000) for 20 mins. Unstained cells and cells staining with only one fluorochrome prepared concomitantly served as control. After one wash in PBS for 5 mins, cells were resuspended in PBS and then sorted with BD FACSARIA II. Nucleated live cells (Hoechst^{+}/APC/Cy7^{-} population) were sorted into PBS with 0.04% BSA for subsequent single-

cell RNA-sequencing.

Single-cell RNA-sequencing

Standard 10x Chromium™ Single Cell 3' v2 (10X Genomics GemCode Technology) protocols were followed for scRNA-seq. Briefly, single cells with specific 10x Barcode and UMI (unique molecular identifier) were generated by partitioning the cells into Gel Bead-In-EMulsions (GEMs). Subsequent cDNA sequences with the same 10x Barcode were considered as sequences from one cell. Library was generated and sequenced with Nova PE150. Sequencing depth was set to be 30 million per cell.

Pre-processing of scRNA-seq Data

Raw sequencing data were demultiplexed, aligned and counted with Cell Ranger pipelines. Basically, "cellranger mkfastq" command was used to generate fastq files, which were leveraged later by command "cellranger count" to produce expression data at a single-cell resolution. "Cellranger aggr" command combines sequencing data from multiple libraries with mapped sequencing depth.

Clustering and Pathway Analysis of scRNA-seq Data

After aggregation of samples from wt and ApoE$^{-/-}$ adventitial cells with mapped sequencing depth, R package "Seurat" was used for gene and cell filtration, normalization, principle component analysis (PCA), variable gene finding, clustering analysis and t-distributed stochastic nearest neighbor embedding (t-SNE). Analysis were performed with default parameters unless otherwise specified. Briefly, matrix containing gene-by-cell expression data from the aggregated library were imported first to create a Seurat object. Cells expressing less than 200 or more than 2500 genes were filtered out for exclusion of non-cell or cell aggregates. Cells with with a percentage of mitochondrial genes more than 0.05 were also filtered out. Data were then log-normalized for subsequent analysis. Principle component analysis were performed for dimension reduction. After calculation with "JackStraw" function, the first 10 principle components were used for clustering analysis. Clusters were visualized with t-SNE. Visualization of gene expression with violin plot, feature plot, dot plot and heatmap was generated with "Seurat" function "VlnPlot", "FeaturePlot", "DotPlot" and "DoHeatmap" respectively. Markers for a specific cluster against all remaining cells were found with function "FindAllMarkers" (only.pos = TRUE, min.pct = 0.25). Differentially expressed genes (P value < 0.01) between two identities were found with "FindMarkers" function. Gene ontology and KEGG pathway analysis were performed with marker genes of each cluster found by "FindAllMarkers" function or enriched genes found by "FindMarkers" function with average log(fold change) > 0.25 on DAVID website and then plotted with R package "ggplot2".

For sub-clustering of the non-immune populations, raw data of these cells were retrieved from the Seurat object containing aggregated expression matrix for creation of a new and separate Seurat object. Similar gene filtration, PCA analysis, clustering, t-SNE and pathway enrichment analysis were then performed. Cell cycle was analyzed by calculating the G1/S and G2/M score which were plotted in a 2D space as described.[15] Briefly, the G1/S and G2/M scores were calculated by subtracting the mean expression value of the 10n nearest neighbors by expression level and detection frequency from the mean expression value of the n genes of the specified gene set.

WGCNA Network Analysis

Weighted gene co-expression network analysis (WGCNA) from R package "WGCNA" was used for identification of highly correlated gene modules. Briefly, adjacency matrix for signed cell correlation network was first created with a soft power set at 9 to allow for scale-free topology. Dissimilarity of topological overlap matrix (TOM) was then used as input for hierarchical clustering of genes. Minimum number of genes included in each module were set to be 30. Total expression of genes within one module shown as verbose boxplot was used to represent the module expression level. Gene correlation network within each module was

visualized with R package “igraph”. Fruchterman-Reingold layout was applied and the size of the node correlated with the gene module membership value of the corresponding gene. Module-trait relationship was calculated with Pearson correlation. For the correlation of modules with a specific cluster, the cluster being assessed was set to be 1 and the value of remaining clusters was set to be 0. Value of wt cells was set as 0 and value for ApoE$^{-/-}$ cells was set as 1 for the analysis of module-trait (genotype: wt or ApoE$^{-/-}$) correlation.

Pseudotime Trajectory Analysis

Pseudotime trajectory analysis was performed with R package “monocle” (version 2.9) with default settings unless otherwise specified. Genes used for pseudotime ordering were taken from the first 1000 (by P value) differentially expressed genes identified by function “differentialGeneTest” with “fullModelFormulaStri” set as “Cluster”. “DDRTree” method was utilized for dimension reduction and cell ordering along the pseudotime trajectory. Branch analysis (branch point 1 and branch point 2) was performed with “BEAM” function. When presenting the significantly changed ($P < 0.01$) genes in the branch point, 6 gene blocks were chosen according to the distinct patterns of gene expression change towards the 2 different cell states. Genes included in GO term “Cytokine activity” or transcription factors (list obtained from transcription factor database[16]) were intersected with the 6 significantly changed gene blocks identified and presented as heatmap.

Ligand-receptor Cellular Communication Analysis

Ligand-receptor pairs were obtained from previously published data.[17] In the analysis, transcriptomic level of ligands or receptors was taken for bioinformatic prediction of potential interactions at the protein level. After intersecting with genes detected, 2174 ligand-receptor pairs were kept (Supplemental Table I). When calculating ligand-receptor interactions, the ligand-receptor pair is counted if both the expression of ligand gene in the ligand cell and the expression of receptor gene in the receptor cell were above 0. Normalized expression data was used in the analysis. Mean number of ligand-receptor interaction between cell types was calculated by dividing the total number of ligand-receptor pairs (all ligand-receptor pairs were used in calculation) by the multiplication of ligand cell number and receptor cell number. The interaction of specific ligand-receptor pair between cell types was the total number of this ligand-receptor pair divided by the multiplication of ligand cell number and receptor cell number. Communication within selected cell types was demonstrated with chord graph generated by R package “circlize”. Color of the link depicted the ligand cell type. Percentage of cells expressing ligand gene (same color of link and cell type) or receptor gene (different color of link and cell type) was also shown in the graph. Same band color at both ends of the link illustrates interaction within this cell type. For a specific cell type (shown as the band of a specific color surrounding the circular graph), its total contribution to ligand-receptor interactions (ratio of its length to the total length of the band) as well as its contribution as ligand or receptor (ratio of the band length (same color as the link – ligand, different color from the link – receptor) to the total length of this color) could also be seen. Heatmap was generated with R package “pheatmap”.

Culture of Adventitial Mesen II Cluster Cells

Adventitia progenitors were cultured *in vitro* as previously specified[18]. Briefly, the adventitia explants from wt and ApoE$^{-/-}$ mice were cultured on gelatin-coated flasks in stem cell medium (DMEM with 10% Embryomax, 10 ng/ml leukemia inhibitory factor, 0.1 mM 2-mercaptoethanol, 100 U/ml penicillin and 100 mg/ml streptomycin). Primary cells were sorted with anti-Sca-1 magnetic beads (Miltenyi Biotec) and a magnetic cell sorting system. Purified cells were passaged at 1:3 upon 80% confluence. Cells within 5 passages after sorting were utilized for subsequent studies.

Quantitative Polymerase Chain Reaction

RNA was extracted with RNeasy mini kit (Qiagen) following standard protocols. QuantiTect Reverse Transcription Kit (Qiagen) was used for reverse transcription. Primers used were as

follows: *Ccl2*, Forward, 5'-TTAAAAACCTGGATCGGAACCAA-3', *Ccl2* Reverse 5'-GCATTAGCTTCAGATTTACGGGT-3'. Fold change of gene of interest was calculated against internal control *GAPDH*. All samples were run in duplicates.

Mouse CCL2 ELISA and Chemokine ELISA Array

Mouse CCL2 ELISA (R&D systems, MJE00) and chemokine array (Qiagen, MEM- 009A) for supernatant of adventitial cells were performed with manufacturer's protocol. First, 50 μL standard, control or adventitial cell culture supernatant at different time points were added to ELISA microplates with 50 μL Assay Diluent and incubated for 2 hours at room temperature. Following washing, 100 μL conjugates were added to each well and incubated at room temperature for 2 hours. 100 μL stop solution was then added after incubation with 100 μL substrate solution for 30 mins. Absorbance was read at 450 nm with wavelength correction at 540 nm within 15 mins.

Trans-well Assay

Migration assays were performed using transwell inserts with 8.0 μm pore membrane filters (Corning). Bone marrow cells (10^5 cells/100 μl serum-free medium) were seeded into the upper chamber, while the bottom chamber contained vascular adventitial mesenchyme cell culture medium with or without CCL2 blocking antibody (R&D, AB-479-NA). Serum free medium served as negative control. After 4h incubation, non-migrating cells on the upper side of the filters were carefully washed and removed using a swab. The migrated cells on the lower surface of transwell filter were fixed in 4% PFA for 10 min and then stained with 1% crystal violet (Sigma, HT90132) for 15 min. Images were acquired using Nikon Eclipse TS100 microscope. Cells were counted in 5 random fields under the microscope for statistical analysis.

En Face Immunofluorescent Staining of Adventitia

The staining protocol was modified from previous publication.[19] Briefly, the adventitia from the thoracic aorta was separated from the media and intima before permeabilization with 0.2% Triton X-100 in PBS for 15min, which was followed by blocking with 5% donkey serum at room temperature in Eppendorf tubes. Primary antibody was diluted 1:100 in PBS with 2% donkey serum over night at 4°C. Following antibodies were used: anti-LYVE1, Abcam, ab14917; anti-PECAM1, BD Biosciences, 553370; anti-RBFOX3, Abcam, ab177487; anti-ACHE, Life-Tech, MA3-042 (Please see the Major Resources Table in the Supplemental Material). After washing with PBS for three times (5 mins each), the adventitia was stained with secondary antibodies (Life Tech, Alexa Fluor) diluted 1:500 in PBS. The nuclei were counterstained with 4′,6-diamidino-2- phenylindole (DAPI). Stained tissue was mounted on slides with image taken with Leica SP5 confocal microscope.

Availability of Data

The scRNA-seq data of wt and ApoE$^{-/-}$ adventitia are available for reproducing the results. The authors declare that all R scripts used to process data are available from the corresponding author if requested.

Statistical Analysis

Data with 5 or more experiment repeats passed KS normality test that determines data normality and the *F*-test that assesses homogeneity of variance. Unpaired and two-tailed student's t test were applied to analyze data between two groups. Data were expressed as mean ± SD (standard deviation) using Graphpad Prism 6 software. Comparisons across multiple groups with 5 experiment repeats per group were assessed with one-way ANOVA test, followed by Bonferroni post-hoc analysis. Comparisons across multiple groups with 3 experiment repeats per group were assessed with Kruskal-Wallis test, followed by Bonferroni post-hoc analysis. Experiments repeats in each group were specified in the figure legends. Appropriate significance was obtained with a relatively small group size. P value < 0.05 was considered statistically different.

Results

Depiction of Adventitial Cellular Landscape with scRNA-seq

In 12-week-old mice, the plasma cholesterol is significantly increased, and the aorta displayed small and sparse atherosclerosis lesions (Supplementary Figure IA and IB). Aorta is isolated after removal of perivascular fat (Supplementary Figure 1A) and then peeled off with no soft connective tissue still attached to the media layer, as demonstrated by nice the co-localization of ACTA2 and DAPI in the media and endothelial layers (Supplementary Figure IC-ID). To characterize the adventitial cellular landscape, we obtained enzymatically dissociated adventitial cells from 12-week-old male wt and ApoE$^{-/-}$ mice and sorted single nucleated live cells (Hoechst^{+}/APC/Cy7^{-}) for scRNA-seq (Figure 1A and Supplementary Figure IE). 2,271 and 3,153 cells from wt and ApoE$^{-/-}$ adventitia respectively were included in subsequent analysis after quality control. Similar mean reads per cell from wt and ApoE$^{-/-}$ adventitia were achieved after aggregating two datasets with "Cell Ranger" to control for comparable sequencing depth (Supplementary Figure IIA). Data integration with canonical correlation allowed for alignment across conditions[20]. Wt and ApoE$^{-/-}$ cells displayed similar number of unique molecular identifiers (nUMIs), comparable number of genes and aligned distribution along the canonical correlation subspace (Supplementary Figure IIB). In addition, *Apoe* expression in ApoE$^{-/-}$ adventitia was significantly downregulated, confirming the genotype (Supplementary Figure IIC). Unbiased clustering performed with Seurat canonical correlation analysis identified 15 clusters as visualized with t-SNE (Figure 1B). Integrated wt and ApoE$^{-/-}$ datasets displayed satisfactory alignment (Figure 1C) in the clustering analysis. In total 15 clusters were singled out with top 20 (by average log(fold change)) markers for each cluster listed in Supplementary Table I. *Ptprc* (encoding pan-hematopoietic marker *Cd45*) was employed to distinguish immune and non-immune cells (Figure 1D and 1E). Major immune populations identified included the monocyte-macrophages (cluster 4, 7, 8 and 14) which featured the expression of *Cd14* and *Cebpb*, the B cells (cluster 1, 10 and 11) which demonstrated high expression of *Cd79a* and *Cd19*, and T cells (cluster 2, 12 and 13) which exhibited high expression of T cell marker *Cd3d* (Figure 1D and 1E). Innate lymphoid cells encompass similar T cell function and demonstrated high expression of *Il1rl1*[21] and *Gata3* (Figure 1F). Other immune cells included natural killer cells (NK) with marker genes *Gzma*, *Gzmb* and *Klrb1c* (Figure 1D and 1F). Of note, although expression of dendritic cell markers *Flt3*, *Zbtb36* and *Itgax* were detected, no dendritic cluster was singled out, with natural killer cell marker *Gzma* highly expressed in the cluster showing the highest percentage of *Itgax* expression (Supplementary Figure III).

Non-immune cells mainly included three clusters (cluster 3, 5 and 15). Clusters 3 and 5 cells both displayed high expression of extracellular matrix proteins (*Col3a1* and *Col14a1* respectively) (Figure 1F). Cluster 5 cells also showed high level of stem cell marker *Ly6a* (encoding *Sca1*) (Figure 1F). It was noteworthy that, marker genes of cluster 3 and 5 cells displayed a heterogeneous bimodal expression pattern with extensive overlap of marker genes which could be seen in the heatmap (Figure 1F). Claster 9 seemed to be composed of erythrocytes/amyloid cells. Cluster 15 cells consisted mainly of vascular lineages including adventitial smooth muscle cells (*Tagln*) and endothelial cells (*Pecam1*) (Figure 1F). Collectively, distinct gene expression patterns across all clusters were observed (Figure 1F) with unbiasedly identified marker genes for each cluster listed in Supplementary Table II. Assignment of putative cell types to clusters was concluded in Figure 1G. Among the identified cell types, mesenchyme cells, T cells and NK cells demonstrated similar fraction in wt and ApoE$^{-/-}$ adventitia, whereas there was an increased fraction of monocyte-macrophages in ApoE$^{-/-}$ adventitia and a resultant decrease of B cell fraction (Figure 1H). Moreover, clustering of separate wt or ApoE$^{-/-}$ dataset and integrated datasets yielded similar assignment of cells to major cell types identified (Supplementary Figure IID), suggesting the robustness of clustering results.

Heterogeneity of Non-immune Cells in the Adventitia

After depicting the transcriptomic landscape of adventitia cells, we next sought to examine the non-immune population. In previous clustering analysis, ECs and SMCs were included in one cluster,

whereas literature supports their distinct identities. Thus, clustering analysis of the non-immune population was performed again with closer inspection to find markers of each sub-cluster relative to the rest of the non-immune population. We aimed to infer the function of each subpopulation. Although adventitial mesenchyme cells received much attention in cardiovascular studies recently[8], scRNA-seq presents an opportunity to examine the adventitial cells unbiasedly without previous selection of marker genes. Seurat-based clustering analysis singled out 6 non-immune clusters from the non-immune population (clusters 3, 5 and 15), which were well-aligned in wt and ApoE$^{-/-}$ cells (Figure 2A and 2B). The marker genes for each cluster were listed in Supplementary Table III. In accordance with previous studies[8, 22], considerable heterogeneity of stem cell markers, such as *Sca1*, *Cd34* and *Tbx18*, and fibroblast markers, including *Ddr2*, *Col1a1* and *Serpinh1* was detected (Supplementary Figure IVA and IVB). Of note, cell proliferation did not serve as a heterogeneity source, as the proliferation markers including Pcna, Mki67 and Mcm2 was not enriched in a specific cluster and the cell cycle analysis did not demonstrate significant difference among all the non-immune clusters (Supplementary Figure IVC and IVD).

Among the six non-immune clusters, Mesen I and Mesen II are the two major clusters, with significantly more cells than the remaining four (Figure 2A). Expression of endothelial markers *Pecam1* and *Cldn5*, adhesion molecules *Icam2* and *Esam*, endothelial cell specific glycoprotein *Tm4sf1* and endothelial angiogenic factor *Egfl7* allowed us to identify non-immune cluster 4 as adventitial endothelial cells (Adv-ECs), possibly from the vasa vasorum (Figure 2C-2E). Similarly, multiple genes (*Myh11*, *Flna*, *Tpm2* and *Acta2*) specific for smooth muscle cells enabled the identification of non-immune cluster 6 as smooth muscle cells (SMCs) (Figure 2C-2E). In addition to adventitial SMCs, however, the medial SMC contamination could not be fully exluded, given that the adventitia was mechanically peeled off the aorta (Supplementary Figure 1E). GO terms analysis was consistent with the cluster identities, with angiogenesis enriched in Adv- ECs, and actin cytoskeleton organization enriched in SMCs (Supplementary Figure V).

After we confidently assigned the putative identities of cluster 4 and 6 to Adv-ECs and SMCs, we continued to explore the identities for the remaining mesenchyme clusters (Mesen I to IV) that were relatively elusive. Various extracellular matrix proteins (*Col15a1*, *Col4a1* and *Sparcl1*) were enriched in Mesen III cluster (Figure 2D and 2E). Importantly, in Mesen III cluster, *Lpl*, which encoded the enzyme lipoprotein lipase was enriched and *Ccl11* also displayed exclusive expression (Figure 2C). Among marker genes of Mesen IV cluster, *Dkk3* demonstrated importance in inducing smooth muscle differentiation[23], *Tbx20* was an essential transcription factor for cardiac development[24], *Prelp* was cartilage-specific[25] and *Ptn* was a heparin-binding cytokine crucial for glial cell differentiation and angiogenesis[26] (Figure 2C-2E). Functional analysis of Mesen IV cluster marker genes also suggested diverse functions of the cells with enriched GO terms “Chondrocyte differentiation”, “Negative regulation of ossification” and “Heart development” (Supplementary Figure V).

Marker genes for Mesen I cluster included *Mfap4*[27] and *Adamtsl2*[28], extracellular matrix proteins important for elastic fiber and microfibril formation (Figure 2C and 2D). *Mfap4* accelerated neointima formation through promoting SMC migration[29] and a similar role of adventitial *Mfap4* might exist. In addition, *Gas6*, whose function in fibrotic diseases such as lung and liver fibrosis had been well-characterized, was enriched in Mesen I cluster (Figure 2D).[30, 31] The enriched GO term “ECM organization” and “Collagen fibril organization” further suggested the role of Mesen I cells in structural organization of adventitia (Supplementary Figure V). Tumor suppressing genes *Igfbp7* and *Pdgfrl* were also highly expressed in Mesen I cluster (Figure 2C and 2E).[32, 33] For Mesen II cluster, stem cell marker *Ly6a*[18] (encoding *Sca1*) and pericyte marker *Cd248*[34] were enriched (Figure 2C-2E). Interestingly, *Ccl2*, a chemokine secreted mainly by inflammatory cells and dysfunctional endothelial cells in atherosclerosis[35, 36], was selectively expressed in Mesen II cluster (Figure 2C). Other enriched genes in Mesen II cluster included *Pla1a*, which was activated in inflammatory conditions[37] and *Pi16*, which was regulated by shear stress and inflammation[38] (Figure 2D). Moreover, apart from *Ccl2*, multiple other genes involved in inflammatory response were enriched in Mesen II cluster, including *Ccl7* and *Anxa1* (Supplementary Figure VIA). Consistently, GO terms (biological function) analysis found enriched GO term “Cell adhesion” with Mesen II

marker genes (Supplementary Figure V).

After investigation of cluster identities, we next sought to examine the changes of adventitial cells in ApoE$^{-/-}$ mice fed on normal laboratory diet in comparison with wt mice, which represented early stage of atherosclerosis. Given the different hemodynamics in the adventitial vasa vasorum and large arteries[39], it was hypothesized that adventitial vasa vasorum endothelial cells might also be dysfunctional in atherosclerosis development, similar to endothelial dysfunction of large arteries. To inspect this hypothesis, *Pecam1* positive non-immune adventitial cells from wt and ApoE$^{-/-}$ mice were compared. GO terms analysis demonstrated enriched chemokine activity, CCR chemokine receptor activity and arachidonic acid binding in ApoE$^{-/-}$ *Pecam1* expressing adventitial cells (Figure 2F), showcasing early changes of adventitial endothelial cells in atherosclerosis.

Collectively, we have identified 6 non-immune clusters (Mesen I to IV, Adv-EC and SMC) from the adventitial non-immune population (cluster 3, 5 and 15). For convenience, markers for cluster identity interpretation mentioned above were summarized in a table (Supplementary Figure VIB). Confident identity assignment was achieved for Adv-ECs and SMCs clusters. Mesen III cluster was important in lipid metabolism according to the transcriptomic profile and Mesen IV cluster displayed potential involvement in chondrocyte development, ossification and heart development. Mesen I and Mesen II clusters, which were the two major clusters, included stem/progenitor cells that had a variety of potentials to differentiate into other cell types and demonstrated potential contribution to adventitia basal structure formation. To further characterize non-immune clusters in the adventitia, we continued to explore the gene expression dynamics and cellular trajectories.

Gene Correlation Dynamics of the Adventitial Non-immune Population

Clustering analysis provided an opportunity to identify clusters and find marker genes of each cluster. However, the gene-gene correlation dynamics (relationship of genes) were neglected. To understand the gene expression dynamics, we employed R package “WGCNA” which utilized the dissimilarity topological overlap among genes to generate gene modules that contained correlated genes which were regulated in a similar mode.[40] The identified gene modules represented distinct cell identities[41] or different cell states related to external traits[42].

In the adventitial non-immune populations, we obtained 13 modules which contained genes to some extent correlated or changed in a similar manner (Figure 3A). Due to the large size (containing 1739 genes), the blue module might contain too many noise genes and was not included in downstream analysis. Correlation analysis of the gene modules with cluster identities revealed that the brown, magenta, cyan, green, salmon and red modules were related to Mesen I, Mesen II, Mesen III, Adv-ECs, Mesen IV and SMCs cluster respectively (Figure 3B). The pink module highly associated with the genotype (wt or ApoE$^{-/-}$) (Figure 3B, last column), with upregulated expression of pink module genes in ApoE$^{-/-}$ adventitial non-immune cells (Figure 3C). As shown by the gene correlation network, *Cxcl2* and *Il1b*[43, 44], two important cytokines in atherosclerosis were included in the pink module (Figure 3D). Interestingly, the correlation of gene modules with Mesen I and Mesen II cluster displayed a highly refined reverse trend, suggesting that these two clusters might be cells at different phases (Figure 3B, first and second columns). Consistent with previous cluster assignment, the green module that highly correlated with Adv-ECs contained mainly endothelial specific genes and the red module that highly correlated with SMCs contained mainly smooth muscle specific genes (Supplementary Figure VII). The greenyellow module was correlated with Mesen III cluster and the most enriched GO term was “Complement activation” (Figure 3B, 3E4 and 3F4). In Mesen IV cluster, associated salmon module displayed highest expression (Figure 3E) and contained genes including *Tbx20*, *Dkk3* and *Wif1* as illustrated in the network (Figure 3F5). In accordance with clustering analysis, these inter-correlated genes displayed similar enriched GO terms as the marker genes of Mesen IV cluster (Figure 3G5).

Although the black module was most correlated with Mesen I cluster, it also displayed high expression in Mesen II and III clusters (Figure 3E1). According to the multiple enriched extracellular matrix genes (*Col1a1*, *Col3a1*, *Col1a2*) in the center of the network and the enriched GO terms (“Collagen fibril organization” and “Protein folding”) (Figure 3F1 and 3G1), it was inferred that Mesen I, Mesen II and Mesen III clusters contributed to the ECM organization in the adventitia. The brown

module genes showed high expression in Mesen I cluster and the hub gene (at the center of the network with highest gene-module membership value) was *Mgp* (encoding matrix Gla protein), a calcification inhibitor[45] (Figure 3E2 and 3F2). Enriched GO terms in the brown module also included "ECM organization", which was in part a confirmation of the brown and black module correlation (Figure 3A and 3G). Magenta module showed a modest high level in Mesen II cluster and the genes in the correlation network included chemokines *Cxcl1* and *Ccl2*, which were included with the enriched GO term "Inflammatory response" (Figure 3E3, 3F3 and 3G3).

To sum up, WGCNA correlation analysis allowed identification of modules containing functionally associated genes and demonstrated the transcriptomic dynamics. The two main Mesen clusters (by cell number, Mesen I and Mesen II) correlated with the brown and magenta module respectively, enabling us to further extend understanding of cluster identity and function. Supported by the most enriched GO terms, the modules were assigned "ECM organization" module and "Inflammatory response" module (Figure 3F2-3F3 and 3G2-3G3).

Pseudotime Trajectory Analysis of Adventitial Non-immune Cells

After investigating biological identities of the Mesen clusters and exploring the transcriptomic dynamics, we continued to inspect the relationships between different Mesen clusters. With pseudotime analysis, the non-immune population was ordered along a trajectory and cells at different states with two branching points were identified (Figure 4A). Adv-ECs, Mesen IV and SMCs were found at one end of the trajectory and Mesen II clusters were found at the other end (Figure 4B). Mesen I and Mesen III clusters lied in the middle of the trajectory (Figure 4B). Expression level of markers for different clusters further confirmed the cluster distribution along the pseudotime trajectory (Supplementary Figure VIII). Literature review presented some adventitia-derived cells as vascular stem/progenitor cells.[24] Thus, we hypothesized that the branch point 1 represented to an extent the differentiation trajectory of adventitia progenitors to vascular lineages including adventitial ECs and SMCs. Analysis of branch point 1 discovered upregulation of both adventitial EC and SMC markers (*Pecam1*, *Acta2 etc.*) (Supplementary Figure IX). The up-regulation of transcription factor *Erg* which was essential for endothelial differentiation further validated the utilization of branch point 1 to recapitulate vascular differentiation mechanism of stem/progenitor cells (Supplementary Figure X).[46]

Since analysis of branch point 1 to some extent resembled the differentiation mechanism, we next took advantage of branch point 2 analysis to gain insight about Mesen II cluster. First, analysis of branch point 2 uncovered upregulated gene blocks (gene block 3-6) towards cell state 2, with Mesen II marker genes *Ccl2*, *Pi16*, *Ly6a* and *Cd248* in block 4 and 5 (Figure 4C). Plotting of *Ly6a* and *Cd248* along the pseudotime trajectory further demonstrated their upregulation when the cells were steered towards Mesen II cluster (Figure 4D). Interestingly, Mesen I marker genes *Pdgfrl* and *Igfbp7* were also in the upregulated gene blocks (block 6) (Figure 4C). Furthermore, most genes involved in the GO term "Cytokine activity" that were significantly changed in branch point 2 analysis were upregulated, among which were the pro-inflammatory cytokines *Ccl2* and *Ccl11*[47] (Figure 4E and 4F).

Collectively, trajectory analysis unraveled the inter-cluster relationship of non-immune sub-populations. At one end of the pseudotime trajectory were the mature cells including ECs, SMCs and Mesen IV cluster. The Mesen II cluster lied at the other end, implying a distinct role of it with other well-differentiated cells. Branching analysis revealed the upregulation of multiple chemokines while the cells were directed towards the inflammatory state.

Transcriptomic Profile of Immune Populations in the Adventitia

After investigating the transcriptomic profiles of adventitial mesenchyme population, we next sought to unravel the transcriptomic heterogeneity of immune cells. The myeloid clusters (clusters 4, 7, 8 and 14) showed distinct gene expression patterns in comparison with the remaining myeloid populations (Figure 5A). Marker genes for cluster 4 included *Clec4d* and *Xcl2* and for cluster 8, feature genes included *Anxa1* and *Wfdc21*. Cluster 4 monocytes demonstrated high expression of pro- atherosclerotic cytokine *Il1b* and its decoy receptor *Il1r2*[48], whereas cluster 8 monocytes

showed high expression of *Adpgk* (encoding ADP-dependent glucokinase) which was important in glycolysis[49] (Figure 5B). Marker genes for cluster 7 included *Ms4a6c* and *Gngt2* (Figure 5A), allowing us to identify it as inflammatory macrophages[50]. Gene used for characterizing alternatively activated macrophage[51] *Lgals3* was seen with the highest expression in cluster 7, further implying its inflammatory role (Figure 5B). Importantly, resident macrophage marker *Adgre1* (encoding *F4/80*) and aortic resident macrophage marker *F13a1* were enriched in both cluster 7 and cluster 14 (Supplementary Figure XIA). M2 macrophage markers *Folr2, Mrc1* (encoding CD206) and *Cbr2* were also exclusively expressed in cluster 14 (Figure 5A and 5B).[52] The pro-atherosclerotic chemokine *Pf4*, *Sepp1* and *C1qa* were also enriched in cluster 14 macrophages, consistent with previous reports[50] (Figure 5A and 5B, Supplementary Figure XIA). Collectively, the evidence implied that cluster 7 was inflammatory macrophages and cluster 14 was resident macrophages[50]. Indeed, GO term analysis revealed that cluster 14 marker genes participated in cadherin-involved cell-cell adhesion and chemokine activity signaling pathways (Figure 5C). Summary of markers used for cluster identification is shown in Supplementary Figure XIB. Next, comparison of wt and ApoE$^{-/-}$ cluster 14 macrophages demonstrated that this cluster might play an important role in leukocyte attraction into the adventitia (Figure 5D). To inspect this, the communication of cluster 14 resident macrophages with other macrophage populations was examined. *Cxcl12*, which was an important anti-inflammatory cytokine was found to have stronger interaction with other macrophage clusters in ApoE$^{-/-}$ adventitia (Figure 5E), suggesting the significance of resident adventitial macrophages in the early stage of atherosclerotic lesion development.

The T cells and ILCs (innate lymphoid cells) (clusters 2, 12 and 13) displayed distinct gene expression patterns (Figure 5F). In comparison with the remaining T cell and ILCs, cluster 2, cluster 12 and cluster 13 featured high expression of *Gramd3* and *Cd2*, *Arg1* and *Lmna*, and *Cd163l1* and *Tmem176b* respectively (Figure 5F). Cluster 2 cells were identified as mixed T cells, with its high expression of specific T cell surface marker *Cd8a* and the lymphocyte transcription factor *Lef1*[53] as well as transcription factor *Klf2* (Figure 5G). Cluster 13 cells expressed high level of *Il17a*, a specific cytokine for Th17 cells, in addition to *Cxcr6* and *Tmem176b* (Figure 5G). Cluster 12 cells showed high expression of *Il1rl1*, an innate lymphoid cell marker[5]. In addition, cluster 12 cells exhibited an ILC2 (type 2 lymphoid cells) phenotype (*Cd3*$^-$/*Il1rl1*$^+$/*Thy1*$^+$/*Il2ra*$^+$)[54], and showed expression of transcription factor *Gata3*, as well as some expression of type 2 cytokines (*Il5* and *Il13*) (Supplementary Figure XIIA). KEGG analysis of cluster 12 ILC2 cells revealed that the enriched KEGG terms included NF-kB signaling and NOD-like receptor signaling which were essential in innate immunity (Figure 5H), further suggestive of the innate lymphoid cell identity.[55, 56] The markers used for cluster identification is summarized in Supplementary Figure XIIB. To further examine whether the potential role of ILCs in the early onset of atherosclerosis, comparison of their gene expression profile between wt and ApoE$^{-/-}$ mice was performed. As exhibited by the GO terms (biological function) analysis, cluster 12 ILC2 cells showed upregulation of genes involved in cellular response to IL1 and oxidant detoxification (Figure 5I) which represented the early changes of ILCs in ApoE$^{-/-}$ adventitia. Detailed characterization of wt and ApoE$^{-/-}$ *Il1rl1* positive ILC2 cells verified the gene expression profile changes in ILC2 population, including the downregulated *Eif3a*, *Jund* and *Serpinb1a* as well as the upregulated *Il1b*, *Fosl2*, *Ltf* and *Cox17* (Figure 5J). Of note, gene *Prdx5* encoding an antioxidant enzyme and multiple gene related to mitochondrial respiration *(Atp5g3*, *Cox17* and *Cox5b*) were upregulated in ApoE$^{-/-}$ *Il1rl1* positive ILC cells (Figure 5K and Supplementary Figure XIII).

Mesen II Interaction with Adventitial Macrophages

Leveraging scRNA-seq, intercellular communication between heterogenous populations has been revealed to shape organ development.[57] The complex interaction of various adventitial cell types and their mediation of atherosclerosis development was evaluated in our study by examination of the transcriptomic level of ligands and corresponding receptors (Figure 6A). Of note, the interactions in our study are computationally predicted rather than biological. In the adventitia, intercellular communication within mesenchyme populations (Mesen I-IV) and between mesenchyme populations and the monocyte-macrophages (Mono-MΦ clusters 4, 7, 8 and 14) were the dominating interactions, suggesting the importance of mesenchyme populations in maintaining

adventitial homeostasis (Figure 6B and Supplementary Figure XIVA). Furthermore, their communication with monocyte-macrophages demonstrated stronger intercellular crosstalk in ApoE$^{-/-}$ adventitia (Supplementary Figure XIVB). Particularly, cells expressing *Cd34* and *Cav1* interacted with *Sell* and *Icam1* expressed by inflammatory macrophages (MΦ 7) respectively, which may potentially modulate leukocyte influx to the adventitia (Supplementary Figure XV).[58, 59]

Further dissection of the interactions revealed that ligand-receptor pairs included in the GO term "Inflammatory response" contributed to the communication between mesenchyme populations (Mesen I-III) and monocyte-macrophages to a similar extent as its contribution to cellular crosstalk within monocyte-macrophages (Figure 6C and Supplementary Figure XVIA). Importantly, stronger cellular interaction reflected by the mean interaction numbers was also observed in ApoE$^{-/-}$ adventitia (Supplementary Figure XVIB). Of note, the cellular interaction calculation robustness was confirmed by the stable interaction pattern when the cell number effect was adjusted (Supplementary Figure XVIC and XVID). Comparable enrichment of "Chemotaxis", "Cytokine" and "Inflammatory response" between the interaction of Mesen II with inflammatory macrophages (MΦ 7) and interaction of Mesen II with resident macrophages (MΦ 14) further indicated the role of Mesen II in "Leukocyte chemotaxis" (Figure 6D). Specificity of the comparable enrichment was confirmed by lower enrichment of "Inflammatory response" between the interaction of Mesen II and Adv-ECs (Supplementary Figure XVII). Mesen II and MΦ 14 exhibited a similar mode in interaction with inflammatory cells in various ligand-receptor pairs that are involved in "Inflammatory response" including *Ccl2-Ccr2* (ligand-receptor) and *Ccl7-Ccr7* (Figure 6E and 6G, Supplementary Figure XVIII). As expected, the ligands from Mesen II cells that pair with inflammatory macrophages (MΦ 7) demonstrated higher enrichment in "Extracellular matrix" in comparison with ligands that pair with resident macrophages (MΦ 14) (Figure 6D).

Ligand-receptor pairs that selectively existed in Mesen II interaction with immune cells mainly involved those with matrix protein as ligands including *Col1a1-Cd44*, *Col1a2-Itgav* and *Timp1-Cd36* (Figure 6F). Ligand-receptor pairs such as *Ccl24-Ccr2* and *C1qa-Lrp1* selectively existed in the interaction of resident macrophages and inflammatory macrophages, suggesting the inflammatory role of resident macrophages (Supplementary Figure XIX). Increased interaction of various ligand-receptor pairs including *Ccl2-Ccr2*, *Ccl7-Ccr2* and *Il1b-Il1r2* between Mesen II and inflammatory cells in ApoE$^{-/-}$ adventitia further implied the participation of Mesen II in early development of atherosclerosis (Figure 6H). Interestingly, various interactions involving matrix proteins as ligand were also increased in Mesen II and inflammatory cell interactions (Figure 6H). Overall, our exploration of intercellular communications suggested a pro-inflammatory role Mesen II cells through interaction with inflammatory cells, particularly inflammatory macrophages, implying the participation of Mesen II in initiating adventitial inflammation in response to elevated blood lipid levels at the early stage of atherosclerosis. Additionally, the top 50 ligand-receptor pairs between all cell types are shown in Supplementary Table IV which might offer insights for researchers interested in further studying inter-cellular communication.

CCL2 Secreted by Adventitial Mesen II Cells Attracts Immune Cells

After unraveling the pro-inflammatory role of Mesen II cluster of adventitial mesenchyme cells, experiments were then performed *in vitro* to investigate their role in attracting immune cells as a proof-of-concept validation. Sca1 (encoded by *Ly6a*) was a frequently used marker for adventitial mesenchyme cells[8] and highly expressed in Mesen II cluster (Figure 2C). Thus, SCA1 positive cells were selectively enriched for separation of Mesen II adventitial cells from the non-immune population. An increasing trend of *Ccl2* was detected in the ApoE$^{-/-}$ adventitial cells (Figure 7A). Additionally, in the supernatant of adventitial Sca1^{+} cells, CCL2 displayed the highest level among other detected chemokines and also a time-dependent upregulation (Figure 7B and 7C). Furthermore, supernatant from adventitial (Mesen II) cell culture media induced bone marrow cell migration, which was attenuated by the CCL2 blocking peptide (Figure 7D and 7E). Taken together, CCL2 was secreted by adventitial Sca1^{+} cells and functioned *in vitro* as a chemoattractant for bone marrow cells. This proof-of-concept study aided to establish the pro-inflammatory role of adventitial Mesen II cluster.

Rare Cell Types Detected by scRNA-seq

In the end, existence of rare cell types in the adventitia was checked. Adventitial lymphatics played a crucial role in the transport of cholesterol from the vessel wall to the blood stream and correlated with the plaque development in the intima.[60] Here in our study, *Lyve1* expressing cells were detected in both wt and ApoE$^{-/-}$ mesenchyme population, although due to their paucity, no distinct cluster was singled out (Figure 8A, cluster identity is indicated in Figure 2A). At the protein level, LYVE1^{+}/PECAM1^{+} lymphatics were seen in the *en face* staining of adventitia (Figure 8B). Negative control stained with IgG controls displayed no positive staining (Supplementary Figure XX). In addition, neuronal markers including *Rbfox3* (encoding *Neun*) and *Ache* (encoding *Acetylcholinesterase*) were detected in the adventitial mesenchyme population (Figure 8C, cluster identity is indicated in Figure 2A). *Rbfox3* is a specific neuronal maker and *Ache* degrades acetylcholine in cholinergic synapses and is involved in hypertension.[61, 62] The existence of neurons in the adventitia was further confirmed with immunostaining of RBFOX3 and ACHE (Figure 8D). Although these rare cells were not identified as separate clusters, validation of their existence in the adventitia could broaden our understanding of adventitia function in atherosclerosis.

Discussion

With scRNA-seq, we unbiasedly depicted the cellular landscape of aortic adventitia, characterized resident and bone marrow-derived cell populations and displayed several rare types of cells, including neurons, innate lymphoid cells and lymphatic endothelial cells. First, we found that a cluster of resident mesenchyme cells expressing stem/progenitor markers could be a source of several maturely differentiated cells, e.g. endothelial and smooth muscle cells. Second, one sub-population of adventitial mesenchyme cells demonstrated a pro-inflammatory role, with the function to attract immune cells to the adventitia through increased interaction of *Ccl2* and its receptors in ApoE$^{-/-}$ mice. Third, resident macrophages in the adventitia seem to be activated at the early stage of hyperlipidemia. Finally, ligand-receptor pair analysis predicted how resident mesenchyme cells interact and attract immune cells *in vivo*. Thus, the information of adventitial cell atlas provided by scRNA-seq could be useful for understanding the roles of a variety of cells in atherogenesis in response to hyperlipidemia.

Examination of the mesenchyme populations in the adventitia unveiled heterogeneity of previously appreciated cell types including Sca-1^{+}, CD34^{+}, Tbx20^{+} stem cell marker positive cells[63] and Ddr^{+} and Thy1^{+} fibroblast marker positive cells[64]. Additionally, heterogeneous adventitial progenitors and fibroblasts seem to display overlap to an extent which prompts caution when interpreting lineage tracing studies exploring function of these cells since the markers selected might only label subpopulation of the adventitial cells.[64] It is noteworthy that enriched GO terms including “Bone development” and “Ossification” suggested a possible role of Mesen IV cluster in vascular calcification, and adventitial cells were found involved in lesion calcification[65]. Intriguing high expression of *Tbx20* in Mesen IV cluster also proposed the involvement of this cluster in cardiomyocyte differentiation. Spontaneous differentiation of CD34 positive adventitial cells towards cardiomyocyte were reported.[66] Taken together, adventitia harboring stem/progenitor cells have a potential to produce several types of mature cells contributing to vascular remodeling and disease development.

For the two main clusters of the adventitial mesenchyme population, Mesen I and Mesen II, extracellular matrix proteins were highly expressed, backing their fundamental function in forming the basic adventitial structure. Furthermore, the WGCNA-identified modules that contained inter-correlated genes demonstrated reverse correlation with Mesen I and Mesen II cluster, supporting the hypothesis that Mesen I and Mesen II possibly represented two phases of one cell type. Similar to the macrophage polarization theory, a pro-inflammatory role of Mesen II population was proposed, which was further supported by the monocle-generated pseudotime trajectory. Validation of this pro-inflammatory role of Mesen II cluster was achieved by confirming the attraction of bone marrow cells in a CCL2-dependent manner. Our study has implied that inter-cellular communication alterations were early events in atherosclerosis development.

In terms of immune cells, previous studies have established their extensive heterogeneity in advanced plaques and revealed the pro-inflammatory role of non-foamy macrophages.[50, 67, 68] Restricting view to the adventitia, the four identified monocyte-macrophage clusters included two macrophage populations: inflammatory macrophage cluster and resident macrophage cluster. Resident population expressed proatherogenic chemokine *Pf4*, consistent with scRNA-seq data from all immune cells of atherosclerotic aorta.[50] In atherosclerosis-prone ApoE$^{-/-}$ adventitia, altered pathways in resident macrophages included cell-cell adhesion, and leukocyte migration, indicating its underlying role in priming adventitia inflammation. With the characterized transcriptomic profile, resident macrophages might be involved in the cell activation in response to hyperlipidemia, which attracts immune cells. In fact, in the adventitia of ApoE$^{-/-}$ mice, increased percentage of monocyte-macrophages were observed in comparison with the wt adventitia.

Tertiary lymphoid organs encompassing T cells, B cells and other types of immune cells were reported to emerge in non-resolving inflammations in aortic adventitia, particularly in the abdominal aorta.[69] Consistently, multiple lymphocyte populations were uncovered in our study. Interestingly, apart from the mixed T cells and Th17 cells, an *Il1rl1* positive cluster was discovered which fit the innate lymphoid cell identity. Importantly, this population did not express pan-T-cell marker *Cd3d* (Figure 1B), basophil marker *Mcpt8*[57] or mast cell marker *Enpp1* (encoding CD203c)[70] (data not shown). Innate lymphoid cells mirror the T cell function and represent a novel avenue in immunology.[21] Protective role of type-2 innate lymphoid cells in peri-vascular adipose tissue implied that this population in the adventitia which was located in more proximity to atherosclerotic lesions might undertake important function in regulating lesion development.[71] Moreover, increased expression of genes related to oxidative phosphorylation in *Il1rl1* positive population in adventitia from ApoE$^{-/-}$ mice fed on normal laboratory diet demonstrated the early modulation of this cell type in atherosclerosis. Function of this previously unrecognized cell type from aortic adventitia in atherosclerosis merits further investigations. As to dendritic cells, no separate cluster was found in our study, possibly suggesting the involvement of dendritic cells in later stages of atherosclerosis as suggested by previous studies[4, 6].

Adding another layer of diversity to the cellular landscape of adventitia, lymphatic endothelial cells and neuronal cells were detected by scRNA-seq despite their rarity. Adventitial lymphatics reversely transport cholesterol and correlate with intimal thickness and thus atherosclerosis progression.[60, 72] Although sensory nerves (including cholinergic nerves characterized by *Ache* expression) have been reported to exist in the adventitia, assisted with scRNA-seq, our study presents as the first one to detect RBFOX3 positive neurons in the adventitia[73], which may be important in vessel contraction.

Altogether, utilization of ApoE$^{-/-}$ mice fed on normal laboratory diet enabled us to characterize the fine-tuned interaction between cells in the adventitia in the early stage of atherosclerosis and uncover early landscape shift of adventitial cells. Interference of these early events bears the potential to prevent or reverse atherosclerotic lesions.

In the end, limitations of our study exist in the following aspects. The first limitation lies in the restricted inclusion of samples. Since our attention was mainly cast on adventitial cells during early stage of atherosclerosis development, only wt and ApoE$^{-/-}$ adventitia from mice fed on normal laboratory diet was examined. Based on primary results from this study, we aim to sequence adventitial cells from other atherosclerotic models (LDLR$^{-/-}$ mice), mice fed on western diet, aging mice and mice with advanced atherosclerotic lesions fed with statin in the future. Secondly, although the number of cells analyzed is sufficient in supporting the analysis in this study, future sequencing of more cells or selective enrichment of a specific population would provide further insight in rare populations in the adventitia. Thirdly, we focused on analyzing the sequencing data in depth, and the *in vitro* experiments served mainly as a proof-of-concept study. Based on the wealth of information provided by the sequencing data, however, extensive *in vitro* experiments could be performed in the future to selectively enrich specific clusters and validate their role (such as ILCs) during atherosclerotic lesion development. Lastly, although we intend to gain a whole view of the adventitial cell atlas without pre-selection of sub-clusters, enzymatical dissociation of single cells induced damage more in branched and large cells and less in small cells like lymphocytes, which

might introduce systematic bias in the study and lead to under-representation of macrophages. *In situ* RNA-sequencing carries the potential to solve this issue.[74] Future research also includes establishment of function in each cell type in atherosclerosis using lineage-tracing models with cluster specific markers.

In summary, adventitia is gradually acknowledged as an essential interface harboring diverse cell types among which both mesenchyme cells and inflammatory cells exist and participate in vascular disease progression. With scRNA-seq, we managed to systematically characterize the cellular landscape of the dynamic adventitia at a single-cell resolution, present interesting populations to study and illustrate a pro-inflammatory sub-population of adventitial mesenchyme cells, which served as a proof-of-concept study for their involvement in early development of atherosclerosis.

Acknowledgements

The authors thank Yaqin Zhang for the sketches of adventitia isolation process.

Sources of funding

This work is supported by the British Heart Foundation (RG/14/6/31144), and National Science Fund for Distinguished Young Scholars (81425002), CAMS Innovation Fund for Medical Sciences (2016-I2M-1-002, 2017-I2M-B&R-02, 2016-I2M-4-003), National Natural Science Foundation of China (81630003), Beijing Natural Science Foundation (7181009).

Disclosures

None.

References

1. Rocha VZ and Libby P. Obesity, inflammation, and atherosclerosis. *Nat Rev Cardiol*. 2009;6:399-409.
2. Campbell KA, Lipinski MJ, Doran AC, Skaflen MD, Fuster V and McNamara CA. Lymphocytes and the adventitial immune response in atherosclerosis. *Circ Res*. 2012;110:889-900.
3. Maiellaro K and Taylor WR. The role of the adventitia in vascular inflammation. *Cardiovasc Res*. 2007;75:640-8.
4. Moos MP, John N, Grabner R, Nossmann S, Gunther B, Vollandt R, Funk CD, Kaiser B and Habenicht AJ. The lamina adventitia is the major site of immune cell accumulation in standard chow-fed apolipoprotein E-deficient mice. *Arterioscler Thromb Vasc Biol*. 2005;25:2386-91.
5. Higuchi ML, Gutierrez PS, Bezerra HG, Palomino SA, Aiello VD, Silvestre JM, Libby P and Ramires JA. Comparison between adventitial and intimal inflammation of ruptured and nonruptured atherosclerotic plaques in human coronary arteries. *Arq Bras Cardiol*. 2002;79:20-4.
6. Houtkamp MA, de Boer OJ, van der Loos CM, van der Wal AC and Becker AE. Adventitial infiltrates associated with advanced atherosclerotic plaques: structural organization suggests generation of local humoral immune responses. *J Pathol*. 2001;193:263-9.
7. Tanaka K, Nagata D, Hirata Y, Tabata Y, Nagai R and Sata M. Augmented angiogenesis in adventitia promotes growth of atherosclerotic plaque in apolipoprotein E-deficient mice. *Atherosclerosis*. 2011;215:366-73.
8. Zhang L, Issa Bhaloo S, Chen T, Zhou B and Xu Q. Role of Resident Stem Cells in Vessel Formation and Arteriosclerosis. *Circ Res*. 2018;122:1608-1624.
9. Majesky MW. Adventitia and perivascular cells. *Arterioscler Thromb Vasc Biol*. 2015;35:e31-5.
10. Hu Y and Xu Q. Adventitial biology: differentiation and function. *Arterioscler Thromb Vasc Biol*. 2011;31:1523-9.
11. Li G, Chen SJ, Oparil S, Chen YF and Thompson JA. Direct in vivo evidence demonstrating neointimal migration of adventitial fibroblasts after balloon injury of rat carotid arteries. *Circulation*. 2000;101:1362-5.

668 12. Kokkinopoulos I, Wong MM, Potter CMF, Xie Y, Yu B, Warren DT, Nowak WN, Le Bras A, Ni Z, Zhou C,
669 Ruan X, Karamariti E, Hu Y, Zhang L and Xu Q. Adventitial SCA-1(+) Progenitor Cell Gene Sequencing Reveals
670 the Mechanisms of Cell Migration in Response to Hyperlipidemia. *Stem Cell Reports*. 2017;9:681-696.
671 13. Roostalu U, Aldeiri B, Albertini A, Humphreys N, Simonsen-Jackson M, Wong JKF and Cossu G.
672 Distinct Cellular Mechanisms Underlie Smooth Muscle Turnover in Vascular Development and Repair. *Circ*
673 *Res*. 2018;122:267-281.
674 14. Robinet P, Milewicz DM, Cassis LA, Leeper NJ, Lu HS and Smith JD. Consideration of Sex Differences
675 in Design and Reporting of Experimental Arterial Pathology Studies-Statement From ATVB Council.
676 *Arterioscler Thromb Vasc Biol*. 2018;38:292-303.
677 15. Biton M, Haber AL, Rogel N, Burgin G, Beyaz S, Schnell A, Ashenberg O, Su CW, Smillie C, Shekhar K,
678 Chen Z, Wu C, Ordovas-Montanes J, Alvarez D, Herbst RH, Zhang M, Tirosh I, Dionne D, Nguyen LT, Xifaras
679 ME, Shalek AK, von Andrian UH, Graham DB, Rozenblatt-Rosen O, Shi HN, Kuchroo V, Yilmaz OH, Regev A
680 and Xavier RJ. T Helper Cell Cytokines Modulate Intestinal Stem Cell Renewal and Differentiation. *Cell*.
681 2018;175:1307-1320 e22.
682 16. Kanamori M, Konno H, Osato N, Kawai J, Hayashizaki Y and Suzuki H. A genome-wide and
683 nonredundant mouse transcription factor database. *Biochem Biophys Res Commun*. 2004;322:787-93.
684 17. Ramilowski JA, Goldberg T, Harshbarger J, Kloppmann E, Lizio M, Satagopam VP, Itoh M, Kawaji H,
685 Carninci P, Rost B and Forrest AR. A draft network of ligand-receptor-mediated multicellular signalling in
686 human. *Nat Commun*. 2015;6:7866.
687 18. Hu Y, Zhang Z, Torsney E, Afzal AR, Davison F, Metzler B and Xu Q. Abundant progenitor cells in the
688 adventitia contribute to atherosclerosis of vein grafts in ApoE-deficient mice. *J Clin Invest*. 2004;113:1258-65.
689 19. Xie Y, Potter CMF, Le Bras A, Nowak WN, Gu W, Bhaloo SI, Zhang Z, Hu Y, Zhang L and Xu Q. Leptin
690 Induces Sca-1(+) Progenitor Cell Migration Enhancing Neointimal Lesions in Vessel-Injury Mouse Models.
691 *Arterioscler Thromb Vasc Biol*. 2017;37:2114-2127.
692 20. Butler A, Hoffman P, Smibert P, Papalexi E and Satija R. Integrating single-cell transcriptomic data
693 across different conditions, technologies, and species. *Nat Biotechnol*. 2018;36:411-420.
694 21. Eberl G, Colonna M, Di Santo JP and McKenzie AN. Innate lymphoid cells. Innate lymphoid cells: a
695 new paradigm in immunology. *Science*. 2015;348:aaa6566.
696 22. Majesky MW, Dong XR, Hoglund V, Mahoney WM, Jr. and Daum G. The adventitia: a dynamic
697 interface containing resident progenitor cells. *Arterioscler Thromb Vasc Biol*. 2011;31:1530-9.
698 23. Karamariti E, Margariti A, Winkler B, Wang X, Hong X, Baban D, Ragoussis J, Huang Y, Han JD, Wong
699 MM, Sag CM, Shah AM, Hu Y and Xu Q. Smooth muscle cells differentiated from reprogrammed embryonic
700 lung fibroblasts through DKK3 signaling are potent for tissue engineering of vascular grafts. *Circ Res*.
701 2013;112:1433-43.
702 24. Stennard FA, Costa MW, Elliott DA, Rankin S, Haast SJ, Lai D, McDonald LP, Niederreither K, Dolle P,
703 Bruneau BG, Zorn AM and Harvey RP. Cardiac T-box factor Tbx20 directly interacts with Nkx2-5, GATA4, and
704 GATA5 in regulation of gene expression in the developing heart. *Dev Biol*. 2003;262:206-24.
705 25. Grover J and Roughley PJ. Characterization and expression of murine PRELP. *Matrix Biol*.
706 2001;20:555-64.
707 26. Deuel TF, Zhang N, Yeh HJ, Silos-Santiago I and Wang ZY. Pleiotrophin: a cytokine with diverse
708 functions and a novel signaling pathway. *Arch Biochem Biophys*. 2002;397:162-71.
709 27. Pilecki B, Holm AT, Schlosser A, Moeller JB, Wohl AP, Zuk AV, Heumuller SE, Wallis R, Moestrup SK,
710 Sengle G, Holmskov U and Sorensen GL. Characterization of Microfibrillar-associated Protein 4 (MFAP4) as a
711 Tropoelastin- and Fibrillin-binding Protein Involved in Elastic Fiber Formation. *J Biol Chem*. 2016;291:1103-
712 14.
713 28. Hubmacher D and Apte SS. ADAMTS proteins as modulators of microfibril formation and function.
714 *Matrix Biol*. 2015;47:34-43.
715 29. Schlosser A, Pilecki B, Hemstra LE, Kejling K, Kristmannsdottir GB, Wulf-Johansson H, Moeller JB,
716 Fuchtbauer EM, Nielsen O, Kirketerp-Moller K, Dubey LK, Hansen PB, Stubbe J, Wrede C, Hegermann J, Ochs
717 M, Rathkolb B, Schrewe A, Bekeredjian R, Wolf E, Gailus-Durner V, Fuchs H, Hrabe de Angelis M, Lindholt JS,
718 Holmskov U and Sorensen GL. MFAP4 Promotes Vascular Smooth Muscle Migration, Proliferation and

719 Accelerates Neointima Formation. *Arterioscler Thromb Vasc Biol*. 2016;36:122-33.
720 30. Rangarajan S and Lee JS. The TAMing of the Idiopathic Pulmonary Fibrosis Myofibroblast. One Step
721 Closer? *Am J Respir Crit Care Med*. 2018;197:1377-1378.
722 31. Barcena C, Stefanovic M, Tutusaus A, Joannas L, Menendez A, Garcia-Ruiz C, Sancho-Bru P, Mari M,
723 Caballeria J, Rothlin CV, Fernandez-Checa JC, de Frutos PG and Morales A. Gas6/Axl pathway is activated in
724 chronic liver disease and its targeting reduces fibrosis via hepatic stellate cell inactivation. *J Hepatol*.
725 2015;63:670-8.
726 32. Rupp C, Scherzer M, Rudisch A, Unger C, Haslinger C, Schweifer N, Artaker M, Nivarthi H, Moriggl R,
727 Hengstschlager M, Kerjaschki D, Sommergruber W, Dolznig H and Garin-Chesa P. IGFBP7, a novel tumor
728 stroma marker, with growth-promoting effects in colon cancer through a paracrine tumor-stroma
729 interaction. *Oncogene*. 2015;34:815-25.
730 33. Kawata K, Kubota S, Eguchi T, Aoyama E, Moritani NH, Oka M, Kawaki H and Takigawa M. A Tumor
731 Suppressor Gene Product, Platelet-Derived Growth Factor Receptor-Like Protein Controls Chondrocyte
732 Proliferation and Differentiation. *J Cell Biochem*. 2017;118:4033-4044.
733 34. Chang-Panesso M and Humphreys BD. CD248/Endosialin: A Novel Pericyte Target in Renal Fibrosis.
734 *Nephron*. 2015;131:262-4.
735 35. Gerszten RE, Garcia-Zepeda EA, Lim YC, Yoshida M, Ding HA, Gimbrone MA, Jr., Luster AD, Luscinskas
736 FW and Rosenzweig A. MCP-1 and IL-8 trigger firm adhesion of monocytes to vascular endothelium under
737 flow conditions. *Nature*. 1999;398:718-23.
738 36. Boring L, Gosling J, Cleary M and Charo IF. Decreased lesion formation in CCR2-/- mice reveals a role
739 for chemokines in the initiation of atherosclerosis. *Nature*. 1998;394:894-7.
740 37. Liu MS, Kang GF and Ghosh S. Activation of phospholipases A1 and A2 in heart, liver, and blood
741 during endotoxin shock. *J Surg Res*. 1988;45:472-80.
742 38. Hazell GG, Peachey AM, Teasdale JE, Sala-Newby GB, Angelini GD, Newby AC and White SJ. PI16 is a
743 shear stress and inflammation-regulated inhibitor of MMP2. *Sci Rep*. 2016;6:39553.
744 39. Ritman EL and Lerman A. The dynamic vasa vasorum. *Cardiovasc Res*. 2007;75:649-58.
745 40. Langfelder P and Horvath S. WGCNA: an R package for weighted correlation network analysis. *BMC*
746 *Bioinformatics*. 2008;9:559.
747 41. Xue Z, Huang K, Cai C, Cai L, Jiang CY, Feng Y, Liu Z, Zeng Q, Cheng L, Sun YE, Liu JY, Horvath S and Fan
748 G. Genetic programs in human and mouse early embryos revealed by single-cell RNA sequencing. *Nature*.
749 2013;500:593-7.
750 42. Langfelder P, Castellani LW, Zhou Z, Paul E, Davis R, Schadt EE, Lusis AJ, Horvath S and Mehrabian M.
751 A systems genetic analysis of high density lipoprotein metabolism and network preservation across mouse
752 models. *Biochim Biophys Acta*. 2012;1821:435-47.
753 43. Bevilacqua MP, Pober JS, Wheeler ME, Cotran RS and Gimbrone MA, Jr. Interleukin-1 activation of
754 vascular endothelium. Effects on procoagulant activity and leukocyte adhesion. *Am J Pathol*. 1985;121:394-
755 403.
756 44. Khan R, Rheaume E and Tardif JC. Examining the Role of and Treatment Directed at IL-1beta in
757 Atherosclerosis. *Curr Atheroscler Rep*. 2018;20:53.
758 45. Bjorklund G, Svanberg E, Dadar M, Card DJ, Chirumbolo S, Harrington DJ and Aaseth J. The role of
759 matrix Gla protein (MGP) in vascular calcification. *Curr Med Chem*. 2018.
760 46. McLaughlin F, Ludbrook VJ, Cox J, von Carlowitz I, Brown S and Randi AM. Combined genomic and
761 antisense analysis reveals that the transcription factor Erg is implicated in endothelial cell differentiation.
762 *Blood*. 2001;98:3332-9.
763 47. Zernecke A and Weber C. Chemokines in atherosclerosis: proceedings resumed. *Arterioscler Thromb*
764 *Vasc Biol*. 2014;34:742-50.
765 48. Garlanda C, Dinarello CA and Mantovani A. The interleukin-1 family: back to the future. *Immunity*.
766 2013;39:1003-18.
767 49. Richter S, Richter JP, Mehta SY, Gribble AM, Sutherland-Smith AJ, Stowell KM, Print CG, Ronimus RS
768 and Wilson WR. Expression and role in glycolysis of human ADP-dependent glucokinase. *Mol Cell Biochem*.
769 2012;364:131-45.

770 50. Cochain C, Vafadarnejad E, Arampatzi P, Pelisek J, Winkels H, Ley K, Wolf D, Saliba AE and Zernecke
771 A. Single-Cell RNA-Seq Reveals the Transcriptional Landscape and Heterogeneity of Aortic Macrophages in
772 Murine Atherosclerosis. *Circ Res*. 2018;122:1661-1674.
773 51. Novak R, Dabelic S and Dumic J. Galectin-1 and galectin-3 expression profiles in classically and
774 alternatively activated human macrophages. *Biochim Biophys Acta*. 2012;1820:1383-90.
775 52. Colin S, Chinetti-Gbaguidi G and Staels B. Macrophage phenotypes in atherosclerosis. *Immunol Rev*.
776 2014;262:153-66.
777 53. Yu B, Zhang K, Milner JJ, Toma C, Chen R, Scott-Browne JP, Pereira RM, Crotty S, Chang JT, Pipkin ME,
778 Wang W and Goldrath AW. Epigenetic landscapes reveal transcription factors that regulate CD8(+) T cell
779 differentiation. *Nat Immunol*. 2017;18:573-582.
780 54. Spits H, Artis D, Colonna M, Diefenbach A, Di Santo JP, Eberl G, Koyasu S, Locksley RM, McKenzie AN,
781 Mebius RE, Powrie F and Vivier E. Innate lymphoid cells--a proposal for uniform nomenclature. *Nat Rev*
782 *Immunol*. 2013;13:145-9.
783 55. Lawrence T. The nuclear factor NF-kappaB pathway in inflammation. *Cold Spring Harb Perspect Biol*.
784 2009;1:a001651.
785 56. Chen G, Shaw MH, Kim YG and Nunez G. NOD-like receptors: role in innate immunity and
786 inflammatory disease. *Annu Rev Pathol*. 2009;4:365-98.
787 57. Cohen M, Giladi A, Gorki AD, Solodkin DG, Zada M, Hladik A, Miklosi A, Salame TM, Halpern KB,
788 David E, Itzkovitz S, Harkany T, Knapp S and Amit I. Lung Single-Cell Signaling Interaction Map Reveals
789 Basophil Role in Macrophage Imprinting. *Cell*. 2018;175:1031-1044 e18.
790 58. Eriksson EE, Xie X, Werr J, Thoren P and Lindbom L. Importance of primary capture and L-selectin-
791 dependent secondary capture in leukocyte accumulation in inflammation and atherosclerosis in vivo. *J Exp*
792 *Med*. 2001;194:205-18.
793 59. Fernandez-Hernando C, Yu J, Suarez Y, Rahner C, Davalos A, Lasuncion MA and Sessa WC. Genetic
794 evidence supporting a critical role of endothelial caveolin-1 during the progression of atherosclerosis. *Cell*
795 *Metab*. 2009;10:48-54.
796 60. Drozdz K, Janczak D, Dziegiel P, Podhorska M, Piotrowska A, Patrzalek D, Andrzejak R and Szuba A.
797 Adventitial lymphatics and atherosclerosis. *Lymphology*. 2012;45:26-33.
798 61. Weyer A and Schilling K. Developmental and cell type-specific expression of the neuronal marker
799 NeuN in the murine cerebellum. *J Neurosci Res*. 2003;73:400-9.
800 62. Lataro RM, Silva CA, Tefe-Silva C, Prado CM and Salgado HC. Acetylcholinesterase Inhibition
801 Attenuates the Development of Hypertension and Inflammation in Spontaneously Hypertensive Rats. *Am J*
802 *Hypertens*. 2015;28:1201-8.
803 63. Yu B, Chen Q, Le Bras A, Zhang L and Xu Q. Vascular Stem/Progenitor Cell Migration and
804 Differentiation in Atherosclerosis. *Antioxid Redox Signal*. 2018;29:219-235.
805 64. Kuwabara JT and Tallquist MD. Tracking Adventitial Fibroblast Contribution to Disease: A Review of
806 Current Methods to Identify Resident Fibroblasts. *Arterioscler Thromb Vasc Biol*. 2017;37:1598-1607.
807 65. Kramann R, Goettsch C, Wongboonsin J, Iwata H, Schneider RK, Kuppe C, Kaesler N, Chang-Panesso
808 M, Machado FG, Gratwohl S, Madhurima K, Hutcheson JD, Jain S, Aikawa E and Humphreys BD. Adventitial
809 MSC-like Cells Are Progenitors of Vascular Smooth Muscle Cells and Drive Vascular Calcification in Chronic
810 Kidney Disease. *Cell Stem Cell*. 2016;19:628-642.
811 66. Mekala SR, Worsdorfer P, Bauer J, Stoll O, Wagner N, Reeh L, Loew K, Eckner G, Kwok CK,
812 Wischmeyer E, Dickinson ME, Schulze H, Stegner D, Benndorf RA, Edenhofer F, Pfeiffer V, Kuerten S, Frantz S
813 and Ergun S. Generation of Cardiomyocytes From Vascular Adventitia-Resident Stem Cells. *Circ Res*.
814 2018;123:686-699.
815 67. Winkels H, Ehinger E, Vassallo M, Buscher K, Dinh HQ, Kobiyama K, Hamers AAJ, Cochain C,
816 Vafadarnejad E, Saliba AE, Zernecke A, Pramod AB, Ghosh AK, Anto Michel N, Hoppe N, Hilgendorf I, Zirlik A,
817 Hedrick CC, Ley K and Wolf D. Atlas of the Immune Cell Repertoire in Mouse Atherosclerosis Defined by
818 Single-Cell RNA-Sequencing and Mass Cytometry. *Circ Res*. 2018;122:1675-1688.
819 68. Kim K, Shim D, Lee JS, Zaitsev K, Williams JW, Kim KW, Jang MY, Seok Jang H, Yun TJ, Lee SH, Yoon
820 WK, Prat A, Seidah NG, Choi J, Lee SP, Yoon SH, Nam JW, Seong JK, Oh GT, Randolph GJ, Artyomov MN,

Cheong C and Choi JH. Transcriptome Analysis Reveals Nonfoamy Rather Than Foamy Plaque Macrophages Are Proinflammatory in Atherosclerotic Murine Models. *Circ Res*. 2018;123:1127-1142.
69. Mohanta SK, Yin C, Peng L, Srikakulapu P, Bontha V, Hu D, Weih F, Weber C, Gerdes N and Habenicht AJ. Artery tertiary lymphoid organs contribute to innate and adaptive immune responses in advanced mouse atherosclerosis. *Circ Res*. 2014;114:1772-87.
70. Tsai SH and Takeda K. Regulation of allergic inflammation by the ectoenzyme E-NPP3 (CD203c) on basophils and mast cells. *Semin Immunopathol*. 2016;38:571-9.
71. Newland SA, Mohanta S, Clement M, Taleb S, Walker JA, Nus M, Sage AP, Yin C, Hu D, Kitt LL, Finigan AJ, Rodewald HR, Binder CJ, McKenzie ANJ, Habenicht AJ and Mallat Z. Type-2 innate lymphoid cells control the development of atherosclerosis in mice. *Nat Commun*. 2017;8:15781.
72. Vuorio T, Nurmi H, Moulton K, Kurkipuro J, Robciuc MR, Ohman M, Heinonen SE, Samaranayake H, Heikura T, Alitalo K and Yla-Herttuala S. Lymphatic vessel insufficiency in hypercholesterolemic mice alters lipoprotein levels and promotes atherogenesis. *Arterioscler Thromb Vasc Biol*. 2014;34:1162-70.
73. Laine P, Naukkarinen A, Heikkila L, Penttila A and Kovanen PT. Adventitial mast cells connect with sensory nerve fibers in atherosclerotic coronary arteries. *Circulation*. 2000;101:1665-9.
74. Chen KH, Boettiger AN, Moffitt JR, Wang S and Zhuang X. RNA imaging. Spatially resolved, highly multiplexed RNA profiling in single cells. *Science*. 2015;348:aaa6090.

Highlights

- Single-cell RNA-sequencing reveals the aortic adventitia as a dynamic interface harboring mesenchyme cells and immune cells including T cells and macrophages.
- Adventitial non-immune cells display significant heterogeneity of progenitor and fibroblast markers.
- A subpopulation of adventitial non-immune cells expressing *Ly6a* attracts immune cells in ApoE$^{-/-}$ mice.
- Ligand-receptor pair analysis predicted how resident mesenchyme cells interact and attract immune cells *in vivo*.

Figure Legends

Figure 1. Identification of main cell clusters in the adventitia of male wt and ApoE$^{-/-}$ mice. (A) Schematic graph of single-cell RNA-sequencing and data analysis pipeline. (B) t-SNE plot of adventitial cells from wt and ApoE$^{-/-}$ mice. Colors denote different genotypes. (C) t-SNE plot of adventitial cells with colors denoting cluster number. (D) Dot plot of selected marker genes for each cluster. (E) Feature plot of markers defining major cell types. (F) Heatmap of the top 20 (by average log(fold change)) marker genes from each cluster and cell type assignment of each cluster. Full list of markers is in Supplemental table II. (G) Cluster and major cell type correspondence. (H) Fraction of each cell type in wt and ApoE$^{-/-}$ adventitial cells. Avg.exp.scale, average scaled expression; pct.exp, percentage of expressing cells; tSNE, t-distributed stochastic neighbor embedding; ILC, innate lymphoid cells; Mono, monocytes; MΦ, macrophage; Eryth, erythrocytes.

Figure 2. Clustering analysis of non-immune cells from wt and ApoE$^{-/-}$ adventitia. (A and B) t-SNE plot of adventitial non-immune cells. Colors denote different clusters (A) or genotype (B). (C) Dot plot of selected marker genes for each non-immune cluster. (D) Violin plot of marker genes of each non-immune cluster. (E) Heatmap of the top 20 (by average log(fold change)) marker genes from each non-immune cluster and cell type assignment. Full list of markers is in Supplemental table III. (F) GO terms (molecular function) analysis of enriched (average log (fold change) > 0.25) genes in ApoeE$^{-/-}$ Pecam1 positive endothelial cells in comparison with the corresponding wild-type cells. Avg.exp.scale, average scaled expression, pct.exp, percentage of expressing cells, exp.scale, scaled expression, cl, cluster, Adv-EC, adventitial endothelial cells, SMC, smooth muscle cells, GOMF, gene ontology molecular function, CCR, C-C chemokine receptor.

Figure 3. Gene expression dynamics of the non-immune population. (A) Eigengene network showing the clustering dendrogram with dissimilarity based on topological overlap and inter-correlation of each module identified by WGCNA. Color indicates modules. Color key indicates the correlation value. (B) Correlation of gene modules with cell cluster identity (Mesen I to IV, Adv-EC and SMC and genotype. Content in each cell represents the correlation value (first row) and the P value (second row). (C) Gene expression distribution of genes from the pink module in wt and ApoE$^{-/-}$ mesenchyme cells were shown by boxplot. (D) GO terms (biological function) analysis of pink module genes. (E) Gene expression distribution of module genes in each mesenchyme cell clusters (Mesen I to IV) were shown by boxplot. (F) Correlation network of the top 20 (by decreasing gene-module membership) genes in each module. Size of the node is in proportion to the gene-module membership, and the length of the link is in reverse correlation with the gene-gene correlation. (G) GO terms (biological function) analysis of genes from each module. Colors indicate the module names. ME, module eigengene; GOBP, gene ontology biological function; ECM, extracellular matrix; IL1, interleukin 1; wt, wild-type.

Figure 4. Pseudotime analysis discovers a pro-inflammatory role of Mesen II cluster. (A) Distinct states of cells identified by pseudotime analysis. (B) Ordering of cells from different non-immune clusters along the pseudotime trajectory. (C) Heatmap of the significantly changed genes ($P < 0.01$) discovered by the "BEAM" function from monocle in branch point 2. (D) Expression level of *Ly6a* and *Cd248* along the pseudotime trajectory. (E) Heatmap showing the expression level of significantly changed genes ($P < 0.01$) in the GO term "Cytokine activity". No significantly changed genes from "Cytokine activity" GO term was found in gene block 2 and 3. (F) Expression level of *Ccl2* and *Ccl11* along the pseudotime trajectory. GO, gene ontology.

Figure 5. Characterization of immune cells from the adventitia. (A-D) Monocyte-macrophages (cl 4, 7, 8, 14). (A) Heatmap of top 20 (by average log(fold change)) marker genes for each monocyte-macrophage cluster in comparison to the rest of the population. (B) Violin plots of selected markers. (C) GO term (molecular function) analysis of cluster 14 macrophages with its marker genes. (D) GO term (biological pathway) analysis of genes significantly upregulated in cluster 14 resident-like ApoE$^{-/-}$ macrophages in comparison to wild-type analogy. (E) Predicted interaction of *Cxcl12* and *Cxcr4* of wt and ApoE$^{-/-}$ macrophages. The same color of link with the cluster indicates that cells from this cluster contribute to the interaction as ligand. Same band color at both ends of the link illustrates interaction within this cell type. (F-K) T lymphocytes and innate lymphoid cells (cl2, 12 and 13). (F) Heatmap of top 20 (by average log(fold change)) marker genes for each cluster relative to the rest of T lymphocytes. (G) Dot plot of selected marker genes for each cluster of T lymphocytes. (H) KEGG analysis of marker genes in cluster 12 innate lymphoid cells. (I) GO terms (biological process) analysis of enriched (average log(fold change) > 0.25) genes in ApoeE$^{-/-}$ cluster 12 innate lymphoid cells in comparison with the corresponding wt cells. (J) Heatmap of top 20 (by decreasing P value) enriched genes ApoE$^{-/-}$ *Il1rl1* positive T lymphocytes compared to corresponding wt cells. (K) Violin plots of selected markers in ApoE$^{-/-}$ *Il1rl1* positive T lymphocytes compared to corresponding wt cells. Cl, cluster; Infla, inflammatory macrophages; Res, resident-like macrophages; GOMF, gene ontology molecular function; GOBP, gene ontology biological pathway; ILC, innate lymphoid cells; exp.scale, scaled expression; wt, wild-type.

Figure 6. Mesen II cells interact with immune cells. (A) Illustration of cell-cell interaction analysis. Ligand is from one cell (same color as the cell) and interacts with receptor from another cell. (B) Mean interaction numbers between cell types from ApoE$^{-/-}$ adventitia. Rows represent ligand cells and columns represent receptor cells. (C) Mean interaction numbers of ligands and receptors from the GO inflammatory response gene set between cell types from ApoE$^{-/-}$ adventitia. Rows represent ligand cells and columns represent receptor cells. (D) Gene set enrichment analysis (UniProtKB Keywords) of the ligands from the top 200 (mean number of interaction) ligand-receptor pairs of ligand cell type (resident MΦ 14 and Mesen II) and receptor cell type (inflammatory MΦ 7). (E) Heatmap of mean interaction numbers of specified ligand-receptor pairs between specified cell types from ApoE$^{-/-}$ adventitia. (F) Heatmap of mean interaction numbers of specified ligand-receptor pairs between specified cell types from ApoE$^{-/-}$ adventitia. (G) Interaction of *Ccl2* and its receptor *Ccr2*, *Ccl7* and its receptor *Ccr2* between ApoE$^{-/-}$ Mesen II, inflammatory macrophages (MΦ 7),

resident macrophages (MΦ 14) and adventitial ECs (Adv-EC) from ApoE$^{-/-}$ adventitia. The same color of link with the cluster indicates that cells from this cluster contribute to the interaction as ligand. (H) Heatmap showing the comparison of mean interaction numbers of specified ligand-receptor pairs between Mesen II and specified cell types from wt and ApoE$^{-/-}$ adventitia. Mesen, mesenchyme; EC, endothelial cell; SMC, smooth muscle cell; wt, wild-type.

Figure 7. Pro-inflammatory role of stromal cells in the adventitia. (A) Gene expression of *Ccl2* in *in vitro* cultured Sca1+ adventitial mesenchyme cells with Gapdh mRNA level as internal control. n = 5. (B) Chemokine array of *in vitro* cultured Sca1+ adventitia mesenchyme cells. n = 3. (C) Protein level of CCL2 in cell culture supernatant detected by ELISA. Time indicates the time for cells in culture. n = 3. Significance determined with Kruskal-Wallis test in comparison with the previous time point was shown. (D) Representative image and correspondent analysis of the migration assay (4 hours) showing the attraction of bone marrow cells by ctrl (serum free medium) and cell culture supernatant (18 hours). n = 5. (E) Representative image and correspondent analysis of the migration assay (4 hours) showing the attraction of bone marrow cells by cell culture supernatant (18 hours) with IgG control or indicated concentrations of CCL2 blocking antibody. n = 5. Significance is determined with one-way ANOVA test. * $P < 0.05$, ** $P < 0.01$, *** $P < 0.001$.

Figure 8. Rare cell types detected by scRNA-seq of the adventitia. (A) Feature plot of lymphatic endothelium markers *Pecam1* and *Lyve1* in wt and ApoE$^{-/-}$ adventitial mesenchyme cells. (B) *En face* staining of wt and ApoE$^{-/-}$ aortic adventitia of PECAM1 and LYVE1. (C) Feature plot of neuronal markers *Rbfox3* and *Ache* in wt and ApoE$^{-/-}$ adventitial mesenchyme cells. (D) *En face* staining of wt and ApoE$^{-/-}$ aortic adventitia for RBFOX3 and ACHE.

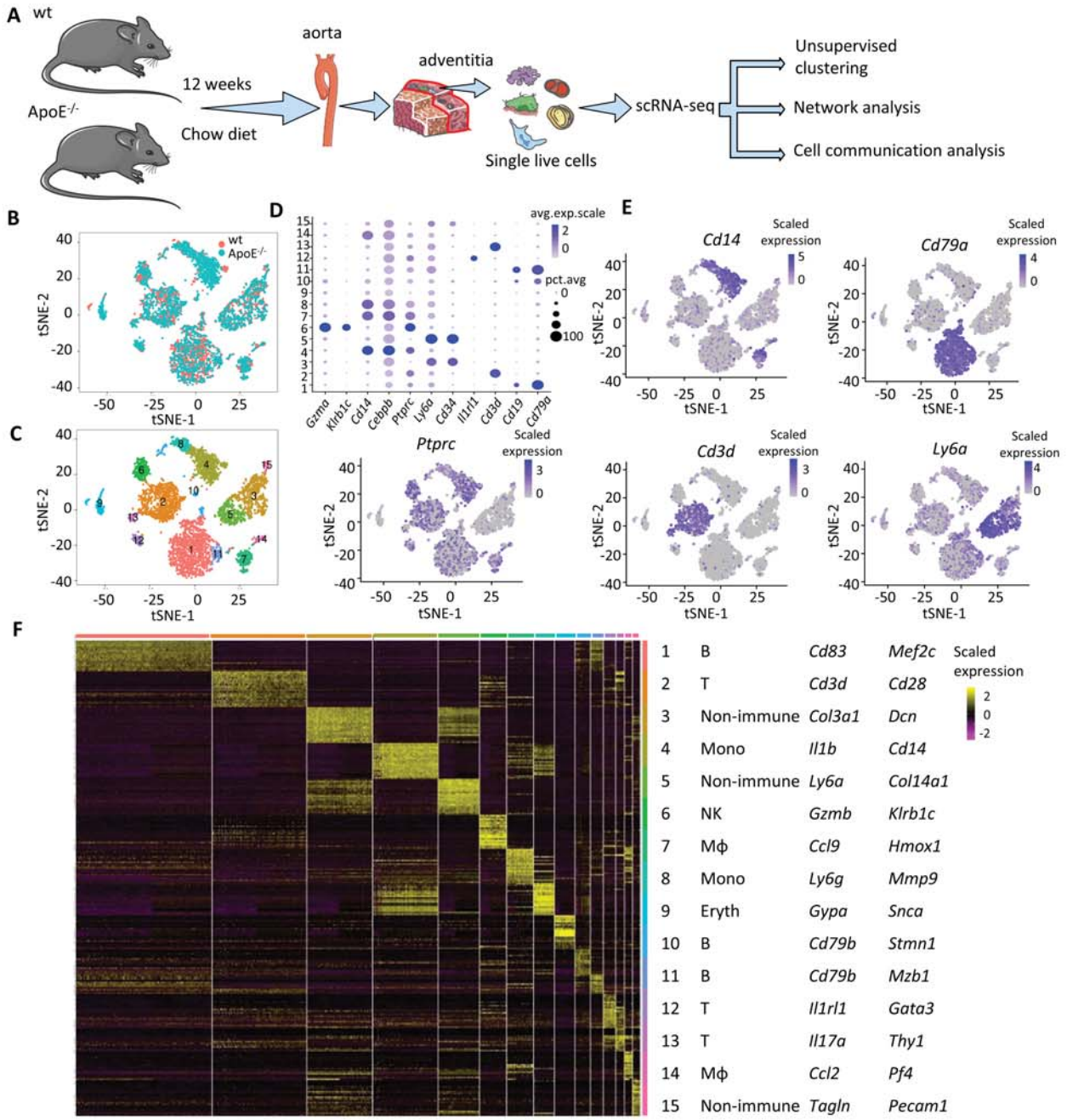

G

Type	Clusters	Markers
Non-immune	3, 5, 15	*Ly6a, Cd34*
T and ILC	2, 12, 13	*Ptprc, Cd3d*
B	1, 10, 11	*Ptprc, Cd19, Cd79a*
Mono-Mϕ	4, 7, 8, 14	*Ptprc, Cd14, Cebpb*
NK	6	*Ptprc, Gzma, Klrb1c*
Eryth	9	*Gypa, Snca*

H

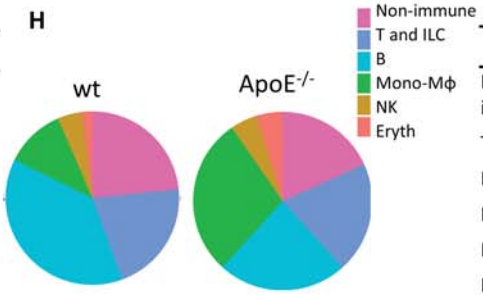

	wt	ApoE-/-
Non-immune	0.233	0.182
T and ILC	0.211	0.201
B	0.378	0.233
Mono-Mϕ	0.112	0.286
NK	0.046	0.049
Eryth	0.019	0.047

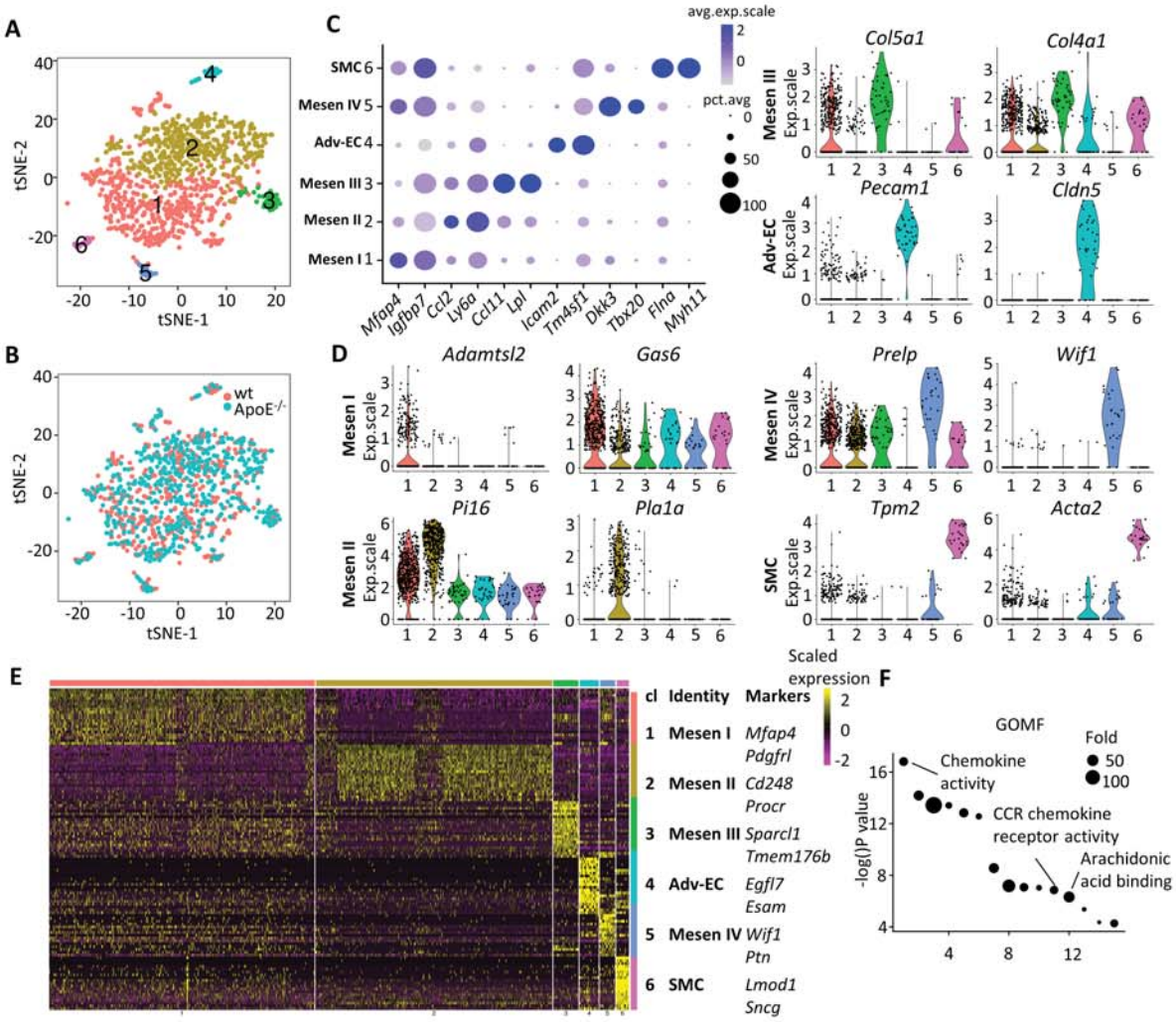
A
tSNE-2
tSNE-1
B
wt
ApoE-/-
C
avg.exp.scale
pct.avg
SMC 6
Mesen IV 5
Adv-EC 4
Mesen III 3
Mesen II 2
Mesen I 1
Mfap4
Igfbp7
Ccl2
Ly6a
Ccl11
Lpl
Icam2
Tm4sf1
Dkk3
Tbx20
Flna
Myh11
Col5a1
Col4a1
Pecam1
Cldn5
Mesen III
Adv-EC
Exp.scale
D
Adamtsl2
Gas6
Prelp
Wif1
Pi16
Pla1a
Tpm2
Acta2
Mesen I
Mesen IV
Mesen II
SMC
Scaled expression
E
cl Identity Markers
1 Mesen I Mfap4 Pdgfrl
2 Mesen II Cd248 Procr
3 Mesen III Sparcl1 Tmem176b
4 Adv-EC Egfl7 Esam
5 Mesen IV Wif1 Ptn
6 SMC Lmod1 Sncg
F
GOMF
Fold
Chemokine activity
CCR chemokine receptor activity
Arachidonic acid binding
-log(P value

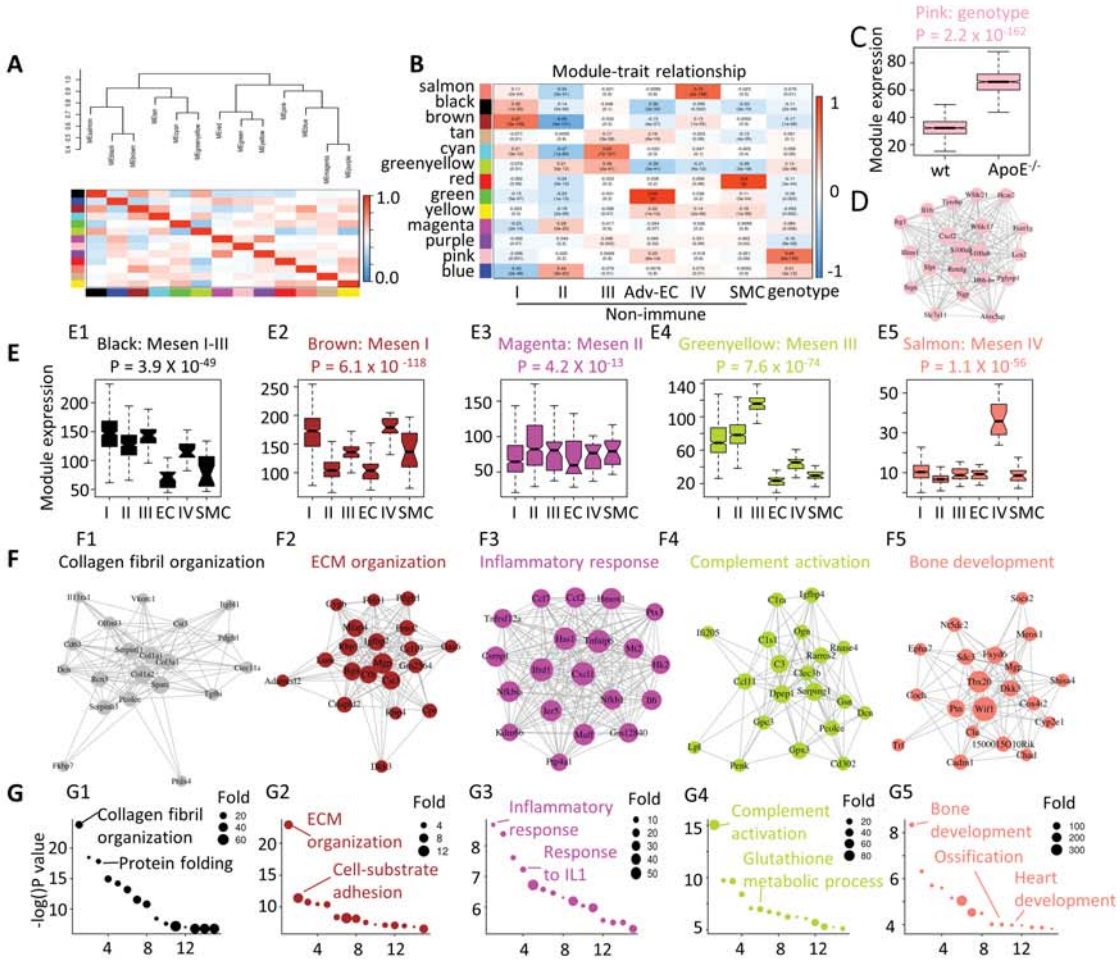
A
B
Module-trait relationship
salmon
black
brown
tan
cyan
greenyellow
red
green
yellow
magenta
purple
pink
blue
I
II
III
Adv-EC
IV
SMC
genotype
Non-immune
C
Pink: genotype
P = 2.2 x 10-162
Module expression
wt
ApoE-/-
D
E
E1
Black: Mesen I-III
P = 3.9 X 10-49
E2
Brown: Mesen I
P = 6.1 x 10-118
E3
Magenta: Mesen II
P = 4.2 X 10-13
E4
Greenyellow: Mesen III
P = 7.6 x 10-74
E5
Salmon: Mesen IV
P = 1.1 X 10-56
F
F1
Collagen fibril organization
F2
ECM organization
F3
Inflammatory response
F4
Complement activation
F5
Bone development
G
G1
Collagen fibril organization
Protein folding
-log()P value
Fold
G2
ECM organization
Cell-substrate adhesion
G3
Inflammatory response
Response to IL1
G4
Complement activation
Glutathione metabolic process
G5
Bone development
Ossification
Heart development

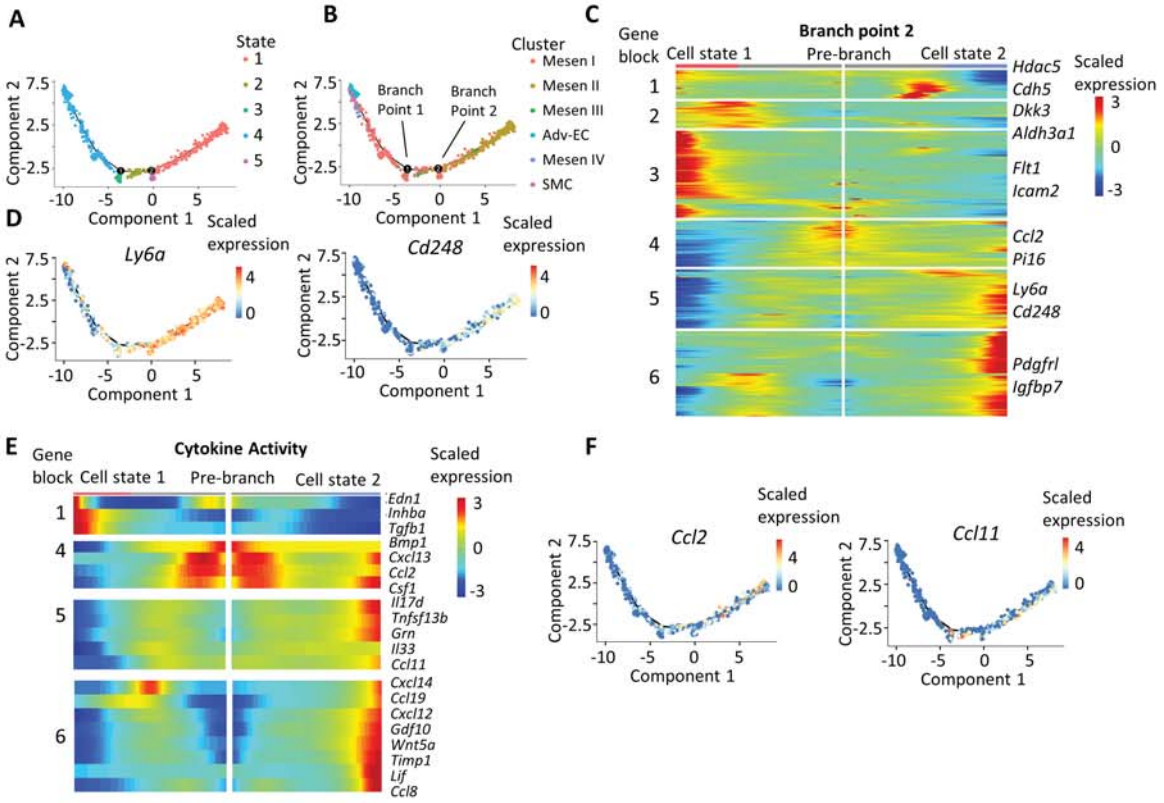
A
State
1
2
3
4
5
Component 2
Component 1
B
Cluster
Mesen I
Mesen II
Mesen III
Adv-EC
Mesen IV
SMC
Branch Point 1
Branch Point 2
C
Branch point 2
Gene block
Cell state 1
Pre-branch
Cell state 2
Scaled expression
Hdac5
Cdh5
Dkk3
Aldh3a1
Flt1
Icam2
Ccl2
Pi16
Ly6a
Cd248
Pdgfrl
Igfbp7
D
Ly6a
Cd248
E
Cytokine Activity
Edn1
Inhba
Tgfb1
Bmp1
Cxcl13
Ccl2
Csf1
Il17d
Tnfsf13b
Grn
Il33
Ccl11
Cxcl14
Ccl19
Cxcl12
Gdf10
Wnt5a
Timp1
Lif
Ccl8
F
Ccl2
Ccl11

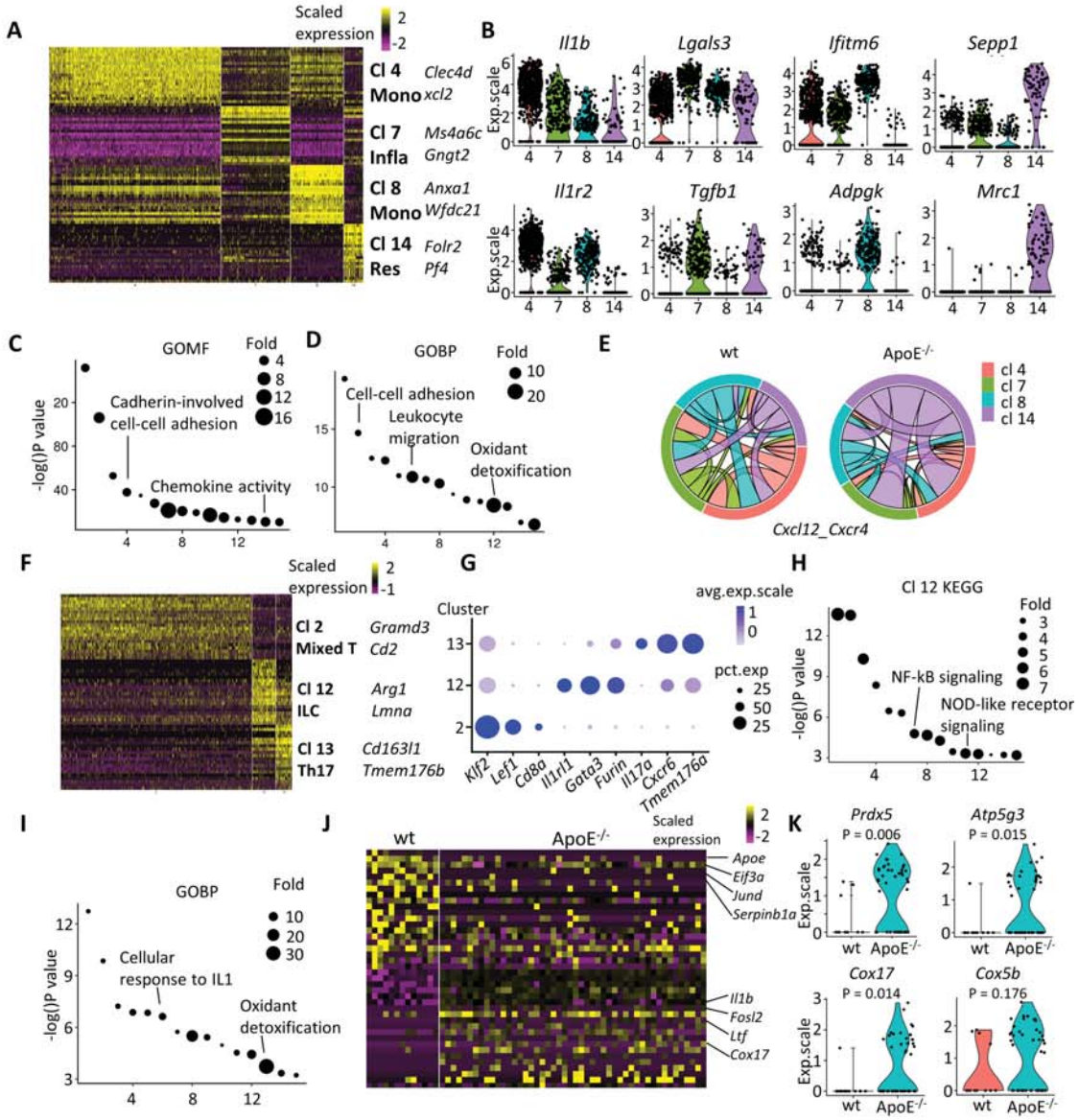
A
Scaled expression
2
-2
Cl 4 Mono
Clec4d
xcl2
Cl 7 Infla
Ms4a6c
Gngt2
Cl 8 Mono
Anxa1
Wfdc21
Cl 14 Res
Folr2
Pf4
B
Il1b
Lgals3
Ifitm6
Sepp1
Il1r2
Tgfb1
Adpgk
Mrc1
Exp.scale
C
GOMF
Fold
4
8
12
16
-log()P value
Cadherin-involved cell-cell adhesion
Chemokine activity
D
GOBP
Fold
10
20
Cell-cell adhesion
Leukocyte migration
Oxidant detoxification
E
wt
ApoE-/-
cl 4
cl 7
cl 8
cl 14
Cxcl12_Cxcr4
F
Scaled expression
2
-1
Cl 2 Mixed T
Gramd3
Cd2
Cl 12 ILC
Arg1
Lmna
Cl 13 Th17
Cd163l1
Tmem176b
G
Cluster
avg.exp.scale
1
0
pct.exp
25
50
25
Klf2
Lef1
Cd8a
Il1rl1
Gata3
Furin
Il17a
Cxcr6
Tmem176a
H
Cl 12 KEGG
Fold
3
4
5
6
7
-log()P value
NF-kB signaling
NOD-like receptor signaling
I
GOBP
Fold
10
20
30
-log()P value
Cellular response to IL1
Oxidant detoxification
J
wt
ApoE-/-
Scaled expression
2
-2
Apoe
Eif3a
Jund
Serpinb1a
Il1b
Fosl2
Ltf
Cox17
K
Prdx5
P = 0.006
Atp5g3
P = 0.015
Cox17
P = 0.014
Cox5b
P = 0.176
Exp.scale
wt
ApoE-/-

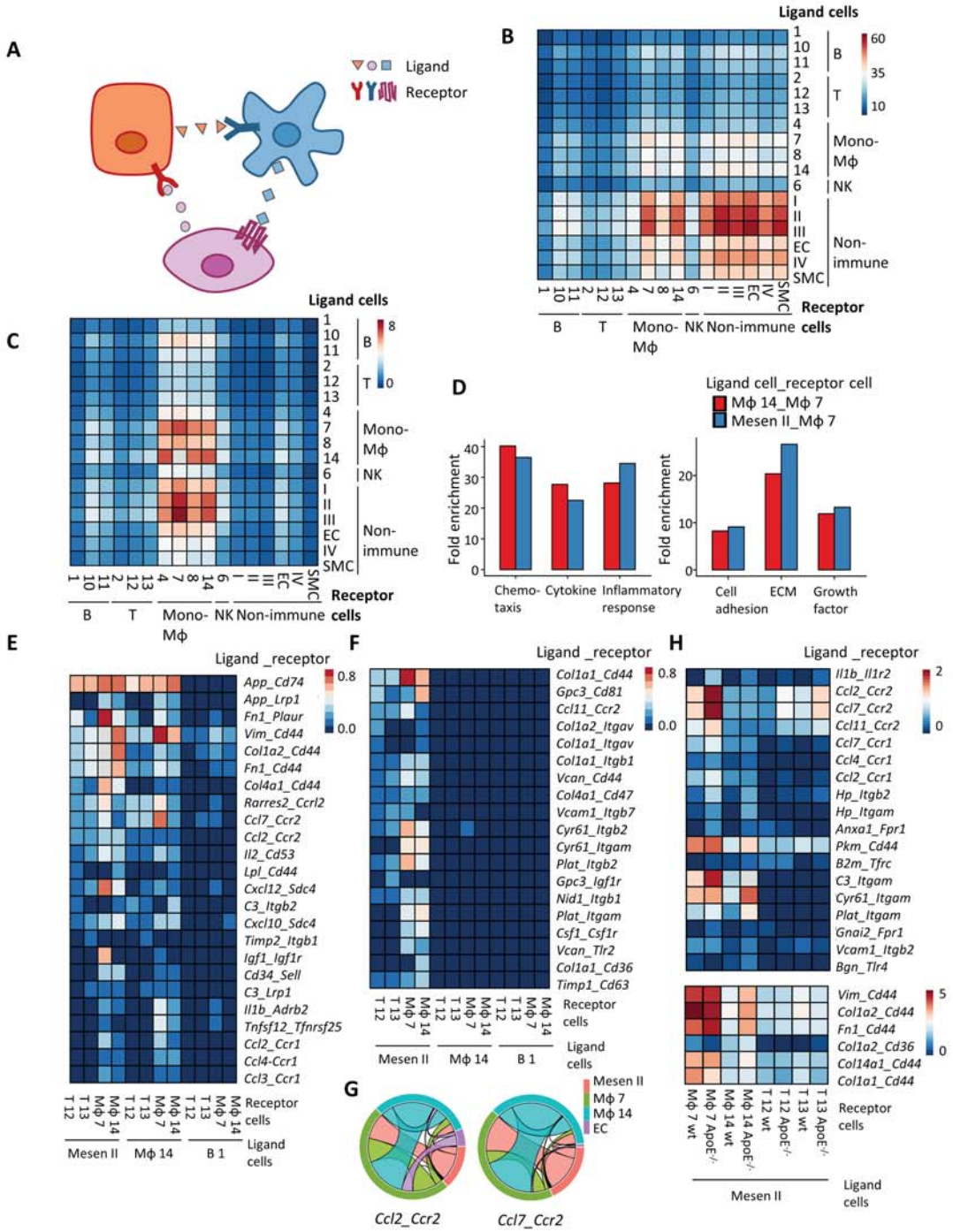
A
Ligand
Receptor
B
Ligand cells
1
10
11
2
12
13
4
7
8
14
6
I
II
III
EC
IV
SMC
B
T
Mono-Mϕ
NK
Non-immune
60
35
10
Receptor cells
C
8
0
D
Ligand cell_receptor cell
Mϕ 14_Mϕ 7
Mesen II_Mϕ 7
Fold enrichment
Chemo-taxis
Cytokine
Inflammatory response
Cell adhesion
ECM
Growth factor
E
Ligand _receptor
App_Cd74
App_Lrp1
Fn1_Plaur
Vim_Cd44
Col1a2_Cd44
Fn1_Cd44
Col4a1_Cd44
Rarres2_Ccrl2
Ccl7_Ccr2
Ccl2_Ccr2
Il2_Cd53
Lpl_Cd44
Cxcl12_Sdc4
C3_Itgb2
Cxcl10_Sdc4
Timp2_Itgb1
Igf1_Igf1r
Cd34_Sell
C3_Lrp1
Il1b_Adrb2
Tnfsf12_Tfnrsf25
Ccl2_Ccr1
Ccl4-Ccr1
Ccl3_Ccr1
0.8
0.0
Receptor cells
Mesen II
Mϕ 14
B 1
Ligand cells
F
Col1a1_Cd44
Gpc3_Cd81
Ccl11_Ccr2
Col1a2_Itgav
Col1a1_Itgav
Col1a1_Itgb1
Vcan_Cd44
Col4a1_Cd47
Vcam1_Itgb7
Cyr61_Itgb2
Cyr61_Itgam
Plat_Itgb2
Gpc3_Igf1r
Nid1_Itgb1
Plat_Itgam
Csf1_Csf1r
Vcan_Tlr2
Col1a1_Cd36
Timp1_Cd63
G
Mesen II
Mϕ 7
Mϕ 14
EC
Ccl2_Ccr2
Ccl7_Ccr2
H
Il1b_Il1r2
Ccl2_Ccr2
Ccl7_Ccr2
Ccl11_Ccr2
Ccl7_Ccr1
Ccl4_Ccr1
Ccl2_Ccr1
Hp_Itgb2
Hp_Itgam
Anxa1_Fpr1
Pkm_Cd44
B2m_Tfrc
C3_Itgam
Cyr61_Itgam
Plat_Itgam
Gnai2_Fpr1
Vcam1_Itgb2
Bgn_Tlr4
Vim_Cd44
Col1a2_Cd44
Fn1_Cd44
Col1a2_Cd36
Col14a1_Cd44
Col1a1_Cd44
2
0
5
Mϕ 7 wt
Mϕ 7 ApoE-/-
Mϕ 14 wt
Mϕ 14 ApoE-/-
T 12 wt
T 12 ApoE-/-
T 13 wt
T 13 ApoE-/-

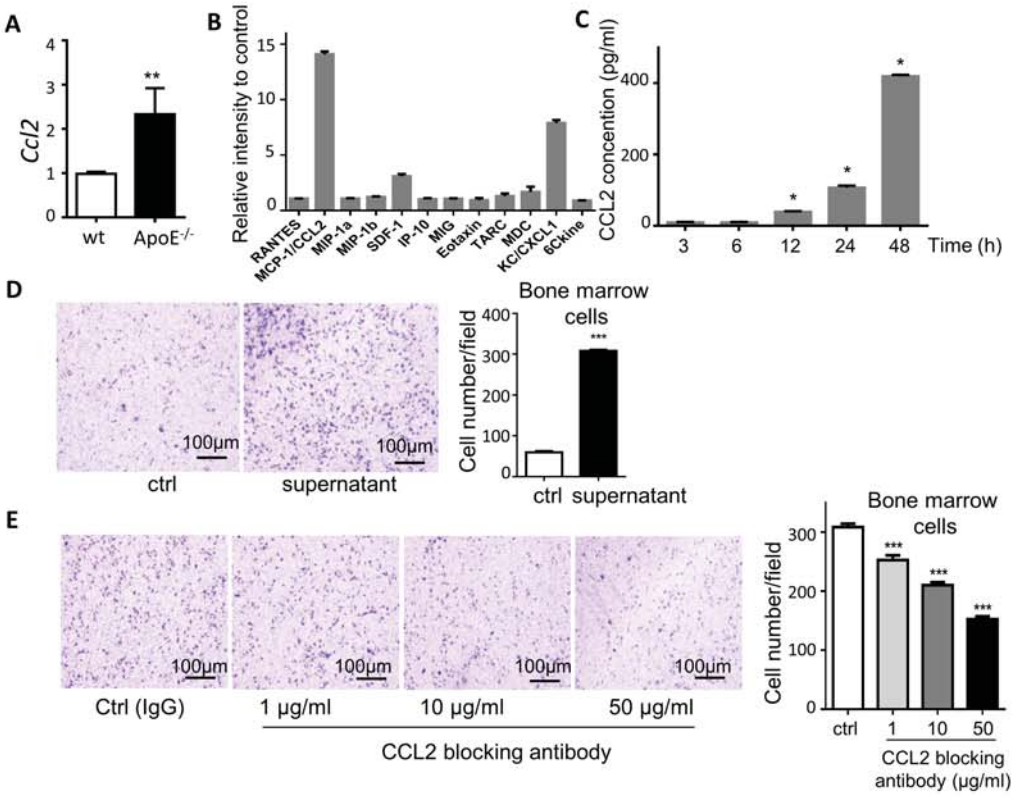
A
Ccl2
wt
ApoE-/-
B
Relative intensity to control
RANTES
MCP-1/CCL2
MIP-1a
MIP-1b
SDF-1
IP-10
MIG
Eotaxin
TARC
MDC
KC/CXCL1
6Ckine
C
CCL2 concention (pg/ml)
Time (h)
D
100μm
ctrl
supernatant
Bone marrow cells
Cell number/field
E
Ctrl (IgG)
1 μg/ml
10 μg/ml
50 μg/ml
CCL2 blocking antibody
CCL2 blocking antibody (μg/ml)

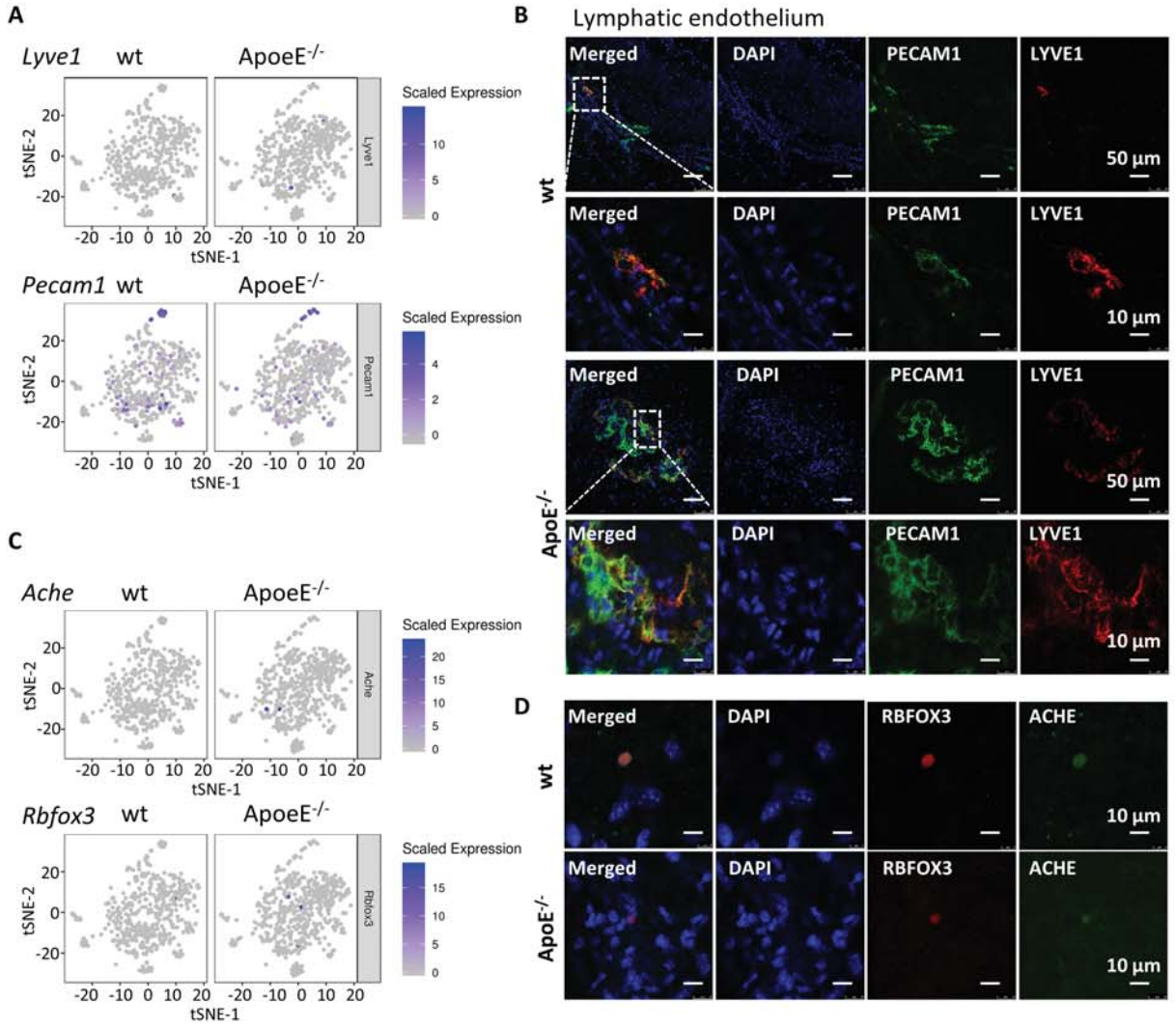
A
Lyve1 wt
ApoeE-/-
Scaled Expression
tSNE-2
tSNE-1
Lyve1
Pecam1 wt
ApoeE-/-
Pecam1
B
Lymphatic endothelium
Merged
DAPI
PECAM1
LYVE1
wt
ApoeE-/-
50 µm
10 µm
C
Ache wt
ApoeE-/-
Ache
Rbfox3 wt
ApoeE-/-
Rbfox3
D
RBFOX3
ACHE